TU-AM-Sym-1 THE CHEMICAL AND MOLECULAR DYNAMICS OF CYTOPLASM IN LIVING CELLS. D. Lansing Taylor, Katherine Luby-Phelps, Gary Bright, Robbin DeBiasio, Lei-Lei Wang and Gregory Fisher. Center for Fluorescence Research in Biomedical Sciences, Carnegie Mellon University, Pittsburgh, PA 15213.

Video enhanced contrast microscopy and quantitative fluorescence microscopy have been employed to define the chemical and molecular dynamics of cytoplasm in Swiss 3T3 cells during wound healing in vitro. The early stages involve the extension of membrane, the polarization of the cells, while the later stages involve cell migration and organelle transport. Size-fractionated fluorescent dextrans and Ficolls have been used to probe the structure of the cytoplasm. Fluorescence recovery after photobleaching (FRAP) of the sized molecules has indicated that some regions of the cytoplasm are composed of a meshwork with an apparent percolation cut-off of ca. 25 nm radius. It is believed that the dynamic meshwork detected by this method plays a role in the cytoskeletal structure of cytoplasm. The ionic properties of cytoplasm in time and space have been explored using ratio imaging microscopy. Cytoplasmic pH has been measured in cells during wound healing and the stimulated cells exhibited spatial variations in ratio values. The involvement of specific proteins in the structure and movement of cytoplasm has also been investigated using fluorescent analogs of actin and myosin. Actin and soluble control molecules rapidly penetrated into newly formed protrusions at the leading edge of cells, while myosin exhibited a lag in appearance within the protrusions. Cell protrusions appear to involve actin assembly followed by the active movement of myosin into the protrusions. Multiple spectral parameter imaging methods have been developed to analyze up to five separate fluorescent probes in the same living cells.

TU-AM-Sym-2 OPTICAL APPROACHES TO THE ANALYSIS OF MOLECULAR DISTRIBUTION IN SINGLE CELLS. F.S. Fay, Dept. of Physiology, University of Massachusetts Medical School, 55 Lake Avenue North, Worcester, MA 01655.

Changes in cell function are believed to result from changes in the cellular levels or distribution of specific molecules. Recent development of highly specific fluorescent probes for proteins, ions and nucleic acids provides the means for directly following changes in the levels and distribution of molecules of interest often in living cells. In my talk I will describe imaging approaches that provide information about molecular distribution with time resolution in msecs. or with 3-D spatial resolution to tenths of a micron. These approaches will be illustrated by results of studies into the role of Ca^{+2} and specific proteins in the contraction of smooth muscle as well as the chemotaxis of neutrophils and esinophils. Supported in part by grants from the NIH (HL14523) and the Muscular Dystrophy Association of America.

TU-AM-Sym-3 THE RESPONSE OF ACTIN GELS TO SHEAR AND ACTIN BINDING PROTEINS. Carl Frieden and Jorge D. Cortese, Department of Biological Chemistry, Washington University School of Medicine, St. Louis, MO 63110.

The properties of actin gels in the presence and absence of actin binding proteins has been investigated. In some experiments we examined the rate of diffusion of different size dextrans or fluorescent beads while in other experiments we used fluorescence photobleaching recovery (FPR) and fluorescence polarization techniques in conjunction with a recently developed cone and plate rotational rheometer. With this device, we are able to measure diffusion coefficients and mobility of actin gels when subjected to either unidirectional or oscillatory shear during polymerization. Using 10% rhodamine labeled actin, we observe microheterogeneity of sheared actin gels both by FPR and by fluorescence polarization experiments. The microheterogeneity appears as different diffusion coefficients and extents of mobility in different areas of the solution subjected to the same shear as well as differences in relaxation processes as measured by polarization fluorescence. By controlling the length of actin filaments with gelsolin (from actin:gelsolin ratios of 100:1 to 300:1) we find that the F-actin diffusion coefficients decrease as the total applied shear increases. This unexpected behavior indicates that the actin filaments are bundling rather than fragmenting at shear rates of 0.05 to 1.3 sec^{-1}. Similar results are observed in unsheared samples in the presence of gelsolin and filamin for actin:filamin ratios of 1:300 to 1:10. Thus the balance between a three-dimensional network and a two-dimensional bundle of filaments appears related to both shear and the presence of actin binding proteins. Supported by DK13332 from the National Institutes of Health.

TU-AM-Sym-4 CONTRIBUTION OF ACTIN TO MECHANICAL PROPERTIES OF MAMMALIAN CORTICAL CYTOPLASM

TP Stossel, JH Hartwig, PA Janmey, KS Zaner, Massachusetts General Hospital and Harvard Medical School.

Actin is believed responsible for viscoelastic properties of cortical cytoplasm. We have never observed elastic behavior in monomeric (G)-actin solutions. Recent measurements of the elastic moduli of polymerized actin (F-actin) (5-6 mg/ml) at low strains reveal high rigidity (250 dynes/cm^2) and nearly fully recoverable strain. Above a critical strain or at lower strains when filaments are shortened by gelsolin, the modulus of F-actin falls markedly and strain recovery diminishes indicative of interpenetrated filaments that are ruptured by shear. Gel-filtered F-actin (GFA) has a very high modulus reducible to that of "conventionally" purified actin by sonically prepared GFA oligomers. F-actin deforms slowly under constant stress, and the deformation rate increases for F-actin shortened by gelsolin or GFA oligomers. The "gel" state of F-actin and especially GFA is thus attributable to effects of filament length which is affected in turn by the presence of factors removed during gel filtration. Actin-binding protein (ABP), which produces orthogonal branching of F-actin in vitro and is immunohistochemically localizable to branch points of filaments in similar actin networks in cortical cytoplasm, markedly increases the rigidity of F-actin (to 8000 dynes/cm^2), elicits strain hardening, a property of living cells, and abolishes creep of F-actin. In contrast to reports concluding that dilute G-actin, semidilute F-actin and F-actin ligated by very different crosslinking molecules are all solids, and a general theory proposing that the viscoelasticity of cortical cytoplasm is attributable to crosslink exchange, we conclude that actin assembly and relatively stable crosslinking are important for cell structure.

TU-AM-MinI-1 STRUCTURE OF THE REACTION CENTER FROM RHODOBACTER SPHAEROIDES R-26 AND 2.4.1; J.P. Allen, G. Feher, U.C.S.D., La Jolla, CA 92093; D.C. Rees, U.C.L.A., Los Angeles, CA 90024

The three dimensional structure of the cofactors and the protein subunits of the RC of the carotenoidless mutant Rb. sphaeroides R-26 was determined by x-ray diffraction at a resolution of 2.8 Å with an R value of 26%[1]. The main features of the structure are similar to the ones determined for R. viridis[2]. Most of the structural features predicted from physical and biochemical measurements are confirmed by the x-ray structure. The structure of the RC from the wild type Rb. sphaeroides 2.4.1 was also determined; the carotenoid was located near $(Bchl)_B$ between the B and C helices of the M-subunit (1) with its axis approximately perpendicular to the two-fold symmetry axis. A structure of the complex formed between cytochrome c_2 and the RC is proposed. The energetics of the membrane-protein interactions were analyzed. The position of the RC in the membrane and the thickness of the membrane were obtained by minimizing the hydrophobic energy with the energy function of Eisenberg and McLachlan. The surface area of the RC is comparable to that of water soluble proteins of similar molecular weight. The volumes of interior atoms are also similar to those of water-soluble proteins, indicating the same compact packing for both types of proteins. The electrostatic potential of the cofactors was calculated. The results show an asymmetry in the potential between the two possible pathways of electron transfer.

(1) J.P. Allen, G. Feher, T.O. Yeates, H. Komiya and D.C. Rees (1987) PNAS, 84, 5730, and 84, 6162; T.O. Yeates, H. Komiya, D.C. Rees, J.P. Allen and G. Feher (1987) PNAS, 84, 6438.
(2) H. Michel, O. Epp and J. Deisenhofer (1986) EMBO J. 5, 2445.

*Work supported by the NSF and NIH.

TU-AM-MinI-2 CALCULATIONS OF SPECTROSCOPIC PROPERTIES AND ELECTRON TRANSFER RATES IN PHOTOSYNTHETIC REACTION CENTERS. W. Parson[a], S. Creighton[b] and A. Warshel[b] (Intr. by J. Fajer), [a]Univ. Washington, Seattle WA 98195, and [b]Univ. Southern California, Los Angeles CA 90007.

It should be possible to use the crystalographic coordinates of the bacterial reaction center to calculate the reaction center's spectroscopic properties and the kinetics of the light-driven transfer reaction. One can start with a molecular orbital treatment of the individual bacteriochlorophyll (BChl) and bacteriopheophytin (BPh) molecules, and treat intermolecular interactions at the level of configuration interactions. Because two of the BChls are very close together, charge-transfer (CT) transitions can mix strongly with local π–π^* transitions, which can result in a large red-shift of the long-wavelength absorption band. Mixing of the local and CT transitions can be analyzed by using semiempirical atomic resonance integrals. This approach accounts well for the absorption, CD and linear dichroism spectra of *Rhodopseudomonas viridis* reaction centers, and explains the sensitivity of the long-wavelength band to external electrical fields. It also yields the interaction matrix elements that govern electron transfer from the special pair of BChls (P) to a BPh. Several mechanisms for electron transfer can be distinguished on the basis of the calculated matrix elements and the energies of intermediate CT states. A mechanism in which an electron first moves from P to another BChl (B) to form P^+B^- as a transient intermediate gives a rate constant close to that found experimentally.

TU-AM-MinI-3 NATURE OF EXCITED STATES IN BACTERIAL PHOTOSYNTHESIS: STARK EFFECT AND PHOSPHORESCENCE
S.G. Boxer, D.J. Lockhart & L. Takiff, Dept. of Chem., Stanford University, Stanford, CA 94305

The magnitude of $|\Delta\mu|$ determined from the Stark effect on the Q_y absorption band of the special pair in Rb. sphaeroides and R. viridis RCs is substantially greater than that for the RC monomer bands or the pure monomeric pigments [1,2]. The Stark effect on the fluorescence spectrum of the Rb. sphaeroides special pair has been measured at 77K. The fluorescence intensity *increases* substantially in an electric field. The magnitude of the second derivative contribution to the ΔF spectrum is *smaller* than that expected for a value of $|\Delta\mu|$ comparable to that observed in absorption [2]. We conclude that: (i) $|\Delta\mu|$ does not increase between the time of excitation and fluorescence (~1–2ps); (ii) $|\Delta\mu|$ may be considerably smaller in fluorescence than absorption; (iii) the rate of initial charge separation can be reduced by application of an electric field.

The phosphorescence spectrum of the triplet state in RCs provides information on the singlet-triplet energy difference in the dimeric special pair. Phosphorescence spectra have been measured for Rb. sphaeroides and R. viridis RCs and for monomeric BChl*a* and *b*. The difference in energy between the fluorescence and phosphorescence maxima (cm^{-1}) are: Rb. sphaeroides, 3370; BChl*a*, 4580; R. viridis, 3130; BChl*b*, 4020. The S–T splitting is smaller for the RCs than for the monomers by 22–26% for both species. We conclude that: (i) the triplet state is not localized on a monomer but is spread somewhat by charge transfer between the two macrocycles comprising the special pair; (ii)the similarity of the S–T splitting for the two species indicates that the degreee of charge transfer character is very similar.

[1]D.J.L. & S.G.B., Biochem., 26,664 (1987); [2]D.J.L. & S.G.B., PNAS, in press.

TU-AM-MinI-4 Free Energy and Temperature Dependence of Intra-Protein Electron Transfer in Photosynthetic Reaction Centers. P. Leslie Dutton, Guillermo Alegria and M.R. Gunner. Dept. Biochem./Biophys., Univ. of Pennsylvania, Phila. Pa 19104

$-\Delta G^{\circ}$ of electron transfer in RCs from Rb. sphaeroides has been changed a)by replacing the native Q_A by quinones with different $E_{\frac{1}{2}}$ values (1,2,3) and b)by applying electric fields to reaction centers in monolayers (4,5). Q_A replacement shows that increasing the $-\Delta G^{\circ}$ for the $Q_A^{\cdot-} \longrightarrow (BChl)_2^{\cdot+}$ electron transfer has little effect on the rate (1);however, decreasing the $-\Delta G^{\circ}$ for this, or for the $BPh^{\cdot-} \longrightarrow Q_A$ reaction, causes the rates to slow (1,2). In no case does the rate become temperature dependent (300 -5K). The rates depend only weakly on Q_A structure and a tail is not required. Both reactions can be modeled with a total reorganization energy (λ) of 600± 100meV and two vibrations (1600 and 150 cm^{-1}); contribution to λ from solvent rearrangement is less than 200meV, implying that the protein provides a reaction medium of low effective dielectric constant. The effect of electric-field induced changes of the $-\Delta G^{\circ}$ on the rate of $Q_A^{\cdot-} \longrightarrow (BChl)_2^{\cdot+}$ electron transfer is also weak, showing general agreement between the two methods. Electric fields appear to have greatest effect on the earliest reactions, involving charge separation between $(BChl)_2$,BChl and BPh; field -induced changes in quantum yield (5) have been interpreted (6) as revealing an electric -field sensitive charge transfer state that precedes the formation of $(BChl)_2^{\cdot+}$ BChl $BPh^{\cdot-}$ Refs. 1)J. Phys. Chem. 90 3783-3795, 2)Gunner and Dutton in preparation. 3)BBA 851 6-22 4)Chem.Phys. 110 227-237 5)BBA 851 38-48 6)Alegria, Gunner and Dutton, this meeting. Supported NSF DMB-85-18433 and DOE-FG02-86ER13476

TU-AM-MinI-5 REACTION CENTER COMPOSITION AND ELECTRON TRANSFER PATHWAYS IN PRIMITIVE PHOTOSYNTHETIC BACTERIA. Robert E. Blankenship, Dept. of Chemistry, Arizona State Univ., Tempe, AZ 85287-1604, USA.

Photochemical reaction center complexes are found in a wide variety of photosynthetic organisms, both prokaryotic and eukaryotic. The reaction centers from these diverse organisms can all be placed into two broad groups, which are distinguished by their electron acceptors. The "quinone type" reaction centers contain a pair of quinone molecules that function as a two-electron gate. Reaction centers with this pattern include Photosystem II from oxygen-evolving organisms, the purple photosynthetic bacteria and the thermophilic green bacterium Chloroflexus aurantiacus. These reaction centers show strong functional similarity, and in many cases this homology is confirmed by amino acid sequence comparisons of the reaction center proteins. The other group of reaction centers, known as the "Fe-S type", is found in Photosystem I, the green sulfur bacteria and the newly-discovered anaerobic bacterium Heliobacterium chlorum. These reaction centers have low potential Fe-S proteins as early electron acceptors, with chlorophyll-type pigments and a quinone as possible earlier acceptors. Some photosynthetic organisms are classed as "primitive" by analysis of their 16 S rRNA. We have analyzed the reaction center composition and kinetic behavior of two of these organisms (Chloroflexus aurantiacus and Heliobacterium chlorum. In Chloroflexus we find that despite considerable differences in the pigment and protein composition, the functional characteristics of the reaction centers are remarkably similar to those of the purple bacteria. Later electron transfer components appear to be less similar to those found in the purple bacteria, but have some similarity to the interchain carriers in oxygen-evolving photosynthetic systems. Analysis of these organisms provides a test of putative structure-function relationships in reaction centers, and may lead to insights into the evolution of photosynthesis. Supported by a grant from the CRGO-USDA.

TU-AM-MinII-1 TRANSFORMING GROWTH FACTOR-ALPHA: STRUCTURE, EXPRESSION AND BIOLOGICAL ACTIVITIES, Rik Derynck, Patricia B. Lindquist, Timothy S. Bringman and M.E. Winkler* Department of Molecular Biology, Genentech, Inc., South San Francisco CA 90480. *Department of Molecular and Biomolecular Chemistry

cDNA analysis has indicated that human TGF-alpha is encoded as an internal part of a 160 amino acid precursor. TGF-alpha synthesizing cells secrete at least two types of glycosylated TGF-alpha in addition to an unglycosylated 50 amino acid form. These different forms are derived by alternative proteolytic cleavage from a transmembrane precursor. The cytoplasmic segment of this precursor is palmitoylated. Immunofluorescent examination of TGF-alpha producing cells shows that TGF-alpha or related molecules are specifically located at the cell surface and that interaction with specific anti TGF-alpha antibodies can result in internalization of the ligand-antibody complex.

The 50 amino acid form was expressed in E. coli. Comparison of TGF-alpha with EGF shows that both molecules interact with the same receptor and exert similar effects. However, TGF-alpha appears to be a superagonist compared to EGF in several biological systems. It can be postulated that TGF-alpha and EGF may interact with the common receptor in a different way which could then be a basis for the observed differences in biological activities.

TU-AM-MinII-2 STRUCTURE-FUNCTION RELATIONSHIPS IN EPIDERMAL GROWTH FACTOR RECEPTOR BINDING. K. H. Mayo, Department of Chemistry, Temple University, Philadelphia, PA 19122.

In this paper, we present experimental data from several sources aimed at attaining some understanding of the forces involved in epidermal growth factor (EGF) receptor binding. Proton NMR spectroscopy has yielded structural information on EGF from three species, i.e.,rat, mouse and human. Since these three species can compete with eachother for cell receptor binding, a common receptor binding domain on EGF is likely. Comparison of these EGF solution conformations has indicated a number of conserved structural regions, one of which may be the receptor binding domain. The spatial arrangement of surface exposed amino acid residues at this binding domain partly defines those forces necessary for efficient receptor association. The complement to these forces must arise from the receptor structure and its cell surface environment. The kinetics and thermodynamics of iodine-125 labelled EGF receptor binding to cultured fibroblast cells, therefore, have been investigated to probe the energetics of this protein-protein interaction. Photo-CIDNP NMR studies of EGFs have identified protein surface exposed aromatic residues which, in the presence of amphipathic micelles, become masked from the polar solvent by the hydrophobic micellar core; different species of EGF interact with these micelles in a similar way. Interestingly, iodine-125 labelled EGF receptor binding data and these micelle interaction data seem to render complementary results. Integration of these data may help define those forces involved in receptor binding.

This research was supported in part by the National Institute of General Medical Sciences (GM-34662) and by the North Atlantic Treaty Organization (NATO) Scientific Affairs Division (RG.85/0424).

TU-AM-MinII-3 THE RECEPTOR FOR EPIDERMAL GROWTH FACTOR. James V. Staros, Vanderbilt University, Department of Biochemistry, School of Medicine, Nashville, TN 37232

The binding of epidermal growth factor (EGF) to its receptor on target cells results in the stimulation of a tyrosyl residue-specific protein kinase. The receptor and the kinase have been shown to be two functional domains of the same molecule, a transmembrane glycoprotein of M_r = 170,000. The stimulation of the activity of the cytoplasmic kinase domain by the binding of EGF to the extracytoplasmic receptor domain appears to be the primary transmembrane signaling event, as abolition of kinase activity results in the loss of cellular responses to EGF. A mechanism will be discussed in which binding of EGF results in an intramolecular conformational change which allows the intermolecular association of two molecules of the receptor/kinase to form a dimeric species with stimulated kinase activity.

Support: NIH DK25489, CA43720

TU-AM-MinII-4 PLATLET DERIVED GROWTH FACTOR RECEPTORS
Rusty Williams, Dept. of Clinical Pharmacology, Univ. of CA, San Francisco, School of Pharmacy, San Francisco, CA

TU-AM-A1 COLLOIDAL CRYSTALS OF PHOSPHOLIPID VESICLES.
Joel A. Cohen, H. Daniel Ou-Yang, and Paul M. Chaikin; Univ. of the Pacific, San Francisco, CA; Univ. of Pennsylvania, Philadelphia, PA; and Exxon Research & Engineering Co., Annandale, NJ.

Colloidal crystals are suspensions of uniformly-sized, uniformly-charged colloidal particles that order spontaneously in deionized solutions. The crystalline arrangements are stabilized by long-range repulsive electrostatic forces, and interparticle distances can be as large as 1 μm. The elastic moduli of these crystals are a function of the particles' intrinsic charge and ionic environment. We have used colloidal-crystal techniques to study the surface electrostatic properties of phospholipid vesicles. Unilamellar PG/PC vesicles were formed in deionized water by high-pressure extrusion through Nuclepore filters. Dynamic light scattering indicated mean vesicle diameters of 0.1 μm and polydispersities of ±20%. Samples of 0.1% to 5% vesicle volume fraction displayed Bragg-like scattering of visible light, and static light-scattering structure factors revealed highly correlated suspensions. Freeze-fracture electron microscopy showed vesicular arrays having short-range order. Shear modulus measurements of 12% samples displayed considerable rigidity. Additions of HCl and KCl reduced the shear moduli continuously to zero, indicative of "glassy" transitions from solid to liquid. These transitions were reversed upon removal of salt. The Poisson-Boltzmann equation was iterated self-consistently from the unit-cell boundary through the vesicle surface to the center of the vesicular shell, permitting calculation of the vesicle surface charge from the shear modulus. The measured salt dependences of the shear modulus thus provide information on phospholipid-protonation and ion-binding phenomena at the vesicle surface.
(Supported in part by NIH grant GM 35241.)

TU-AM-A2 LAMELLAR GEL-LAMELLAR LIQUID CRYSTAL PHASE TRANSITION OF DIPALMITOYLPHOSPHATIDYLCHOLINE MULTILAYERS FREEZE-DRIED FROM AQUEOUS TREHALOSE SOLUTIONS. P.J. Quinn, King's College, London, U.K., R.D. Koynova, B. G. Tenchov, Bulgarian Academy of Sciences, Sofia, Bulgaria, L.J. Lis, Kent State University, Kent, OH.

The mechanism of the phase transition of dipalmitoylphosphatidylcholine multilayers freeze-dried from the fully hydrated gel phase ($L_{\beta'}$) in the presence of trehalose has been investigated by real-time X-ray diffraction methods. Sequential diffraction patterns were recorded with an accumulation time of 3s during heating and 1.2s during cooling between about 20° and 80°C. A transition is observed in the range of 47°-57°C and involves structural events typical of a lamellar gel-lamellar liquid crystal ($L_{\beta'}$-L_α) transformation. This transition is completely reversible with a temperature hysteresis of 2-3°C and thereby resembles the main phase transition of fully hydrated dipalmitoylphosphatidylcholine multilayers. The mechanism of the transition from $L_{\beta'}$ to L_α as seen in the wide-angle scattering profiles show that the sharp peak at about 0.41nm, characteristic of the gel phase, decreases in intensity, broadens and shifts progressively to about 0.44nm towards the end of the transition. A temperature jump of 6°C.s^{-1} through the phase transition region of a freeze-dried dipalmitoylphosphatidylcholine: trehalose mixture (molar ratio 1:1) showed that the phase transition had a relaxation time of about 2s similar to that of the main transition in the fully hydrated lipid. Static X-ray diffraction studies of the melting of dipalmitoylphosphatidylcholine freeze-dried from the lamellar-gel phase in the absence of trehalose showed a transition above 70°C which proceeds by a different mechanism. The low-angle diffraction data of phospholipid:trehalose mixtures are consistent with an arrangement of trehalose molecules in a loosely packed "monolayer" separating bilayers of phospholipid. Trehalose appears to reduce the direct interbilayer hydrogen bond coupling thereby modifying the thermal stability and the phase transition mechanism of the bilayers.

TU-AM-A3 PHASE TRANSITION SEQUENCES AND MECHANISMS FOR DIPALMITOYLPHOSPHATIDYLCHOLINE IN ETHANOL/WATER SOLUTIONS. L.J. Lis, Kent State University, Kent, Ohio; P.J. Quinn, King's College, London, U.K.; and I.W. Levin, NIH, Bethesda, MD.

Dipalmitoylphosphatidylcholine (DPPC) has been shown to form interdigitated bilayer phases when in contact with ethanol-water solutions when greater than 50mg of ethanol per ml of water is present (S.A. Simon and T.J. McIntosh (1984) *Biochim. Biophys. Acta* 773, 169-172). DPPC phases and transitions have been characterized using x-ray diffraction and differential scanning calorimetry for samples with ethanol concentration greater and less then 50mg/ml water. When 10mg ethanol/ml water is used, DPPC bilayers undergo the usual sequence of phases involving the subgel, gel, rippled and liquid crystalline bilayers. However, when a solution of 150mg ethanol per ml water is used, then an interdigitated phase is present in the subgel and gel states. The DPPC phase sequence thus evolves as subgel (interdigitated) to gel (interdigitated) to liquid crystalline bilayers. Preliminary calorimetric examination indicates that there is no hysteresis in the single transition observed for this sample upon multiple heating scans. The mechanism of the gel (interdigitated) to L_α phase transition can also be inferred from real time x-ray diffraction measurements obtained as the sample is undergoing a scan of approx. 8°/min. These studies clearly describe the structural implications of high ethanol concentrations on DPPC bilayers.

TU-AM-A4 PHASE STRUCTURES AND TRANSITIONS FOR DIPALMITOYLPHOSPHATIDYLCHOLINE IN NON-AQUEOUS SOLVENTS. L.J. Lis, W. Tamura-Lis, P.D. Zajak and D. Patterson, Kent State University, Kent, Ohio; P.J. Quinn, King's College, London, U.K.; and J.M. Collins, Marquette University, Milwaukee, WI.

The mesophase structure and acyl chain packing of dipalmitoylphosphatidylcholine can be mediated by the presence of non-aqueous solvents. Samples have been examined using DSC and x-ray diffraction in which water has been totally substituted by a variety of organic or inorganic solvents. For example, the presence of fused salt (ethylammonium nitrate-EAN) was shown to induce a phase sequence for DPPC, as described by x-ray diffraction, which terminated with the formation of an H_{II} phase when the acyl chains transformed from a crystalline bilayer directly to a liquid crystalline bilayer. Characteristic calorimetric scans were produced which were indicative of a second order phase transition when coupled to real time x-ray diffraction data obtained for a similar temperature scan. The sample was further observed to form a gel type bilayer phase after cooling from the H_{II} phase. Similar effects were observed for DPPC in propylene carbonate but not for DPPC in ethylene glycol, dimethyl sulfoxide or nitromethane. These results indicate that cryoprotectants are effective because they tend to stabilize the bilayer phase in lipid and membrane systems and do not induce the formation of non-bilayer phases even above the acyl chain melting temperature.

TU-AM-A5 X-RAY DIFFRACTION AND CALORIMETRY STUDIES OF HYDRATED 1-HEXADECYL, 2-PALMITOYL-sn-GLYCERO-3-PHOSPHOCHOLINE (HPPC). N. Haas, P.K. Sripada, and G.G. Shipley. Biophysics Institute, Boston University School of Medicine, Boston, MA 02118

While hydrated dipalmitoyl phosphatidylcholine (DPPC) forms tilted chain $L_{\beta'}$ bilayers in the gel phase, dihexadecyl phosphatidylcholine (DHPC) exhibits gel phase polymorphism. At low hydrations DHPC forms $L_{\beta'}$ phases but at >30% H_2O a chain-interdigitated gel phase is observed. In this study we report the behavior of a PC with both types of chain linkage, HPPC. HPPC has been investigated as a function of hydration using differential scanning calorimetry (DSC) and x-ray diffraction. By DSC, over the hydration range 12.0 - 70.3 wt% H_2O, HPPC exhibits two reversible transitions. The reversible main chain-melting transition decreases from 44.0°C reaching a limiting value of 38.7°C at full hydration. A shoulder is observed on the low temperature side of the main transition. Incubation at low temperatures (-8°C or -12°C) results in additional sub-transitions indicative of the formation of ordered-chain sub-gel phases. X-ray diffraction patterns of hydrated HPPC (20.9, 27.6, and 52.0 wt% H_2O) have been recorded at 20°C. At the two lower hydrations HPPC exhibits diffraction patterns characteristic of bilayer gel phases (20.9% H_2O, d = 60Å; 27.6% H_2O , d = 63Å) similar to those of the gel phase of DPPC. In contrast, at 52.0 wt% H_2O, HPPC shows a much reduced bilayer periodicity, d = 47Å, and a single sharp reflection at 4.0Å in the wide angle region. This diffraction pattern is identical to that exhibited by the interdigitated phase of DHPC. Therefore, in the gel phase HPPC undergoes a hydration-dependent conversion from a regular bilayer structure to an interdigitated bilayer arrangement. Clearly, the presence of a single ether-linkage (at the sn-1 position) is sufficient to allow formation of the chain-interdigitated phase.

TU-AM-A6 PHYSICAL PROPERTIES AND MOLECULAR PACKING OF 1,2-DIACYL-sn-GLYCEROLS. Dharma R. Kodali, David Fahey, Donald M. Small, Biophysics Institute, Boston Univ.Schl.Med.,Boston, MA 02118

1,2-diacyl-sn-glycerols (sn-1,2 DGs) play a central role as secondary messengers and lipid intermediates. The molecular packing in different polymorphic forms of optically active saturated monoacid sn-1,2 DGs (acyl chain length C_{12}, C_{16}, C_{18}, C_{22}, and C_{24}) were studied by DSC, x-ray diffraction and vibrational spectroscopy and compared to 1,3 analogues. For all the sn-1,2 DGs the solvent-crystallized form melted with a single sharp endotherm. The melting temperatures, enthalpy and entropy of this transition increased with chain length. This solid phase is β' with orthorhombic perpendicular chain packing (wide angle diffraction = 4.3Å^{-1}, 4.0Å^{-1}, and 3.8Å^{-1}), Raman spectra (1421 Cm^{-1}) and infrared absorption (729 and 720 Cm^{-1}). On quenching from the melt the C_{12}, C_{16}, and C_{18} formed a hexagonally packed (4.1Å^{-1}) α-phase which converts to β'-phase when α- melts. On quenching C_{22} and C_{24} a pseudo-hexagonal (4.1Å^{-1} and 3.8Å^{-1}) sub α-phase bilayer is formed. This phase converts to an α-phase before melting. Both α- and β'-forms are bilayer structures. The corresponding saturated monoacid 1,3-diacylglycerols do not form α- or β'-phases. Rather they form solvent-crystallized β_1- and melt crystallized β_2-forms. Both are a triclinic parallel, tilt from the base plane 79° and 68° respectively and have glycerol region thickness of ∿ 7.5Å. In contrast the sn-1,2 DGs in the α and β' forms have chain tilts and glycerol thickness of 90° and 66°, and 9Å and 7Å respectively. Thus the sn-1,2 DGs have quite different crystal structures and polymorphism compared to their 1,3 isomers.

TU-AM-A7 THERMAL TRANSITIONS OF PHOSPHATIDYLCHOLINES ON THE SURFACE OF LIPOPROTEIN-LIKE EMULSION PARTICLES. Donald M. Small, John W. Steiner, Arie Derksen, Susanne Bennett Clark. Biophysics Institute, Boston University School of Medicine, Boston, MA 02118

Biologic emulsions, found in the cytoplasm of cells and as plasma lipoproteins, consist of a core of neutral lipid and a surface of phospholipid with varying amounts of protein and free cholesterol. We examined the transitions of saturated phosphatidylcholines (DMPC, DPPC, DSPC) present in ∿1000Å emulsion particles. Emulsions were made by brief sonication of the phospholipid with triolein and varying amounts of cholesterol. They were fractionated by centrifugation and sized by electron microscopy; transitions were recorded in a Microcal-2 as a function of surface cholesterol concentration. In the absence of cholesterol DSPC and DPPC show sharp transitions corresponding to chain melting of the phospholipid at 51° and 39°C respectively, but no pre-transition. DMPC shows a broad transition at 23°C. Compared to liposomes all the transitions are broad with a calculated cooperative unit of ∿20-25 molecules, compared to ∿100 for liposomes. The enthalpy of the transitions of the phospholipids on emulsions is ∿95% (DSPC), ∿60% (DPPC), and ∿5% (DMPC) of the enthalpy of the same transition in liposomes. This suggests that DMPC interacts most and DPSC least with core molecules. As cholesterol is added to the surface from 0-mol% to 50-mol% the transition broadens; enthalpy decreases and disappears at ∿30 mol% for DSPC and less for DPPC and DMPC. Using these particles as substrates for lipoprotein lipase shows that a solid surface completely abolishes the ability of the enzyme to hydrolyze core molecules. Thus monolayers of phospholipid emulsifiers have transitions at emulsion surfaces and the physical state of the phospholipid may be important in the metabolism of such particles.

TU-AM-A8 CUBIC PHASE IN DOPE. E. Shyamsunder, P.T.C. So, M.W. Tate, D.C. Turner and S.M. Gruner, Physics Department, Princeton University, Princeton, NJ 08544

The L_α-H_{II} phase transition of dioleoylphosphatidylethanolamine (DOPE) in excess water has been extensively studied by many groups. The transition is observed to occur rapidly when a DOPE dispersion is heated from 2°C, where the L_α phase is stable, to 15°C where the H_{II} phase is stable. We report on the induction of a crystallographically well-defined cubic lattice which is slowly formed when the lipid dispersion is rapidly cycled between -5°C and 15°C hundreds of times. Once formed, the cubic lattice is stable at 4°C for weeks. X-ray diffraction indicates that the cubic lattice is most consistent with either the Pn3m or Pn3 space groups. Tests of lipid purity after induction of the cubic indicate the lipid is at least 99% pure. The cubic lattice can be destroyed and the system largely reset by thermally cycling the specimen several times between -30°C and 2°C. The kinetics of the formation of the cubic are dependent upon the rate of temperature change, the overall water concentration and the extreme temperatures of the cycle. At 50% water (wt/wt), which is excess water for both the L_α and H_{II} phases of DOPE, a distinct cubic lattice is obtained in 500 cycles. At 65% water, several thousand cycles induces disorder but no distinct cubic lattice. At 30% water, only well-ordered L_α and H_{II} phases are seen even after thousands of cycles. The presence of stable/metastable cubic phases may be a general feature of H_{II} forming lipids and is discussed in terms of the spontaneous curvature radius of the lipid monolayers (Gruner, Proc. Natl. Acad. Sci. 82 (1985) 3665). Supported by NIH grant GM32614 and DOE grant DE-FG02-87ER60522.

TU-AM-A9 ELECTRON DIFFRACTION STRUCTURE ANALYSIS OF GLYCEROLIPID LAMELLAR PACKING, D.L. Dorset, Electron Diffraction Dept., Medical Foundation of Buffalo, Inc., 73 High St., Buffalo, N.Y. 14203.

Lamellar (00ℓ) electron diffraction intensity data are easily obtained from epitaxially crystallized 1,2-diacyl glycero-lipids for which the long molecular axes are parallel to the largest crystal face. Ab initio quantitative structure analyses can be carried out successfully via a variety of phasing techniques including: (a) translational searches based on molecular conformers found in x-ray crystal structures, (b) analyses of one-dimensional Patterson functions, (c) swelling experiments with hydrated specimens maintained in a low temperature sample holder, or (d) analyses of phase contrast e.m. "lattice images". Examples of successful structure determinations include a series of ether-linked phospholipids: DHPE, DHPEM and DHPC. One of two crystal forms of DHPEM is an interpenetrating chain structure. Phase transitions of these phospholipids can be studied in this orientation as well as the structure of polydisperse layers in conjunction with DSC measurements. Crystal packings of chiral and racemic lipids (e.g. DMPE) can also be compared. For glycerides, the α_L-form of 1,2-dipalmitin was shown not to retain the molecular conformation of the β'_L-form, i.e. the glycerol carbon backbone is perpendicular rather than parallel to the layer surface. In all cases, the orthogonal projection found in electron diffraction patterns from solution crystallized samples can be used separately to determine the methylene subcell and tilt of the long chain axes to the surface plane. The lamellar structure analyses, furthermore, are no less accurate than comparable x-ray determinations. Research supported by a grant from the Manufacturer's & Traders Trust Company.

TU-AM-A10 THE RIGID $Ca(PS)_2$ PHASE BETWEEN BILAYERS FORMS AT LOW Ca^{2+} CONCENTRATIONS IN PS/PC MODEL MEMBRANES. G.W. Feigenson, Section of Biochemistry, Molecular and Cell Biology, Clark Hall, Cornell University, Ithaca, NY 14853

Ca^{2+} binds between phosphatidylserine (PS) lamellae to form a very stable phase of composition $Ca(PS)_2$. For pure palmitoyloleoyl PS (POPS), the equilibrium Ca^{2+} concentration for the formation of $Ca(PS)_2$ is .042 μM. In a mixed lipid system of palmitoyloleoyl phosphatidylcholine (POPC), POPS, Ca^{2+}, and buffer, the same chemical equilibrium is found, i.e.

$$Ca(PS)_2 + \text{water} = Ca^{2+}(aq) + 2PS^-(aq), \qquad K_D = (a_{Ca^{2+}})(a_{PS})^2 / a_{Ca(PS)_2}$$

The thermodynamic activity of $Ca(PS)_2$ is a constant, that of Ca^{2+} is approximated as its concentration in the buffer, and the activity of the PS is given by the mole fraction of PS in the PS/PC mixture multiplied by an activity coefficient. We use ESR and x-ray diffraction to detect the formation of $Ca(PS)_2$, and calcium chelator dyes to measure the aqueous Ca^{2+} concentration. The experimental finding is that the equilibrium Ca^{2+} concentration for $Ca(PS)_2$ formation varies as the inverse square of the PS mole fraction at high PS concentration (Raoult's Law) and as the inverse square of the PS mole fraction multiplied by a constant at low PS concentration (Henry's Law). For example, the equilibrium Ca^{2+} concentration is .12 μM at POPS/POPC = .6/.4, and is 10 μM at POPS/POPC = .2/.8. Such Ca^{2+} concentrations are found in the cytoplasm of stimulated cells, leading to the suggestion that the Ca^{2+}-induced phase transition observed in these simple model systems could have a biological role.

TU-AM-A11 POLYMORPHIC PHASE BEHAVIOR OF LYSOPALMITOYL PHOSPHATIDYLCHOLINE IN POLYETHYLENE GLYCOL-WATER MIXTURES. Martin D. King and Derek Marsh, (Intr. by J. K. Zimmerman) Max-Plank-Institut fur biophysikalische Chemie, Abteilung Spektroskopie, D-3400 Gottingen, Fed. Rep. Germany.

The polymorphic phase behavior of 1-palmitoyl-2-lyso-sn-glycero-3-phosphocholine dispersions in excess water has been studied as a function of temperature and polyethylene glycol (PEG) concentration, using proton-dipolar decoupled ^{31}P NMR spectroscopy and turbidity measurements. At low PEG concentrations (0-12 wt%), a thermotrophic transition occurs at 3-5 °C with increasing temperature, from an interdigitated lamellar gel (L_{β}^I) phase to a normal micellar phase. At intermediate PEG concentrations (12-20 wt%), thermotrophic transitions take place from the lamellar gel phase to a fluid cubic (Q_{α}) phase, and then at higher temperatures from the cubic to the micellar phase. At intermediate PEG concentrations (20-30 wt%), thermotrophic transitions take place from the lamellar gel phase to the cubic phase, then from the cubic phase to a normal hexagonal (H_I) phase, and finally at higher temperature from the hexagonal phase to the micellar phase. At high PEG concentrations (>30 wt%), a thermotrophic transition takes place with increasing temperature from the lamellar gel phase directly to the fluid hexagonal phase. At these high PEG concentrations, the micellar phase is not attained within the accessible temperature range (<80°C). A pseudo-binary phase diagram has been constructed as a function of PEG concentration, and comparison with the phase diagram of lysopalmitoyl phosphatidylcholine as a function of water content (Arvidson et al., Eur. J. Biochem. 152 (1985) 753-759), demonstrates that PEG controls the polymorphic phase behaviour by reducing water activity. This work has been supported in part by the grant Ma 756/2-3 from the Deutsche Forschungsgemeinschaft.

TU-AM-A12 PRECIPITATION OF CALCIUM INSOLUBLE SALTS FROM BILE SALT DISPERSIONS. D. Lichtenberg[1,3], N. Younis[1], E. Werker[1], A. Bor[1] and S. Nir[2] (sponsored by J.W. Ogilvie), Department of Physiology and Pharmacology, Tel Aviv University School of Medicine, Tel Aviv[1], Faculty of Agriculture, Hebrew University of Jerusalem, Rehovol[2], ISRAEL and Department of Biochemistry, University of Virginia School of Medicine, Charlottesville, Virginia 22908[3].

Precipitation of calcium deoxycholate $Ca(DOC)_2$ upon mixing of $CaCl_2$ and NaDOC is rapid only when [DOC] exceeds its cmc (~1.5mM). The rate of precipitation of $Ca(DOC)_2$ from mixtures of Ca^{2+} and DOC micelles is fastest at a [DOC] which depends upon $[Na^+]$. The effect of $[Na^+]$ depends upon $[Ca^{2+}]$ and [DOC]. These results can be rationalized by a model in which precipitation involves Ca^{2+}-induced aggregation of DOC micelles (with Na^+ reducing Ca^{2+}-binding, but increasing the rate of aggregation through surface-charge-neutralization) followed by structural reorganization within the aggregate. An important factor in determining the precipitation rate is the Ca^{2+} to DOC binding ratio. Since other bile salts reduce $Ca(DOC)_2$ precipitation by supressing crystal growth, this process is unlikely in bile and can not be regarded as a potent nucleating factor for cholesterol precipitation. Ca^{2+}-induced precipitation of palmitate (Pal) from mixtures of NaPal and various bile salts occurs through a similar mechanism as it depends similarly on $[Ca^{2+}]$ and $[Na^+]$. The kinetics of $Ca(Pal)_2$ is critically dependent on the ratio of Pal to bile salt anions (i.e. on the number of Pal ions in a bile salt micelle). At fixed $[Ca^{2+}]$, $[Na^+]$ and [bile salt], a slight increase in [Pal] has a dramatic effect on the rate of $Ca(Pal)_2$ precipitation. This underlines the possible role of free fatty acid content (thus, phospholipase activity) in bile in governing the process of gallbladder stone formation.

TU-AM-B1 AN ESR CONTRIBUTION TO THE NEUROMODULATORY ROLE OF TRACE AMINES. J. Harris, S. Trivedi & B. L. Ramakrishna, Arizona State University, Chemistry Department, Tempe, AZ 85287-1604

An ESR study was initiated to examine the concept of a neuromodulatory role of trace amines as suggested by Boulton. Isolated rat brain synaptosomal membranes were labelled with nitroxide positioned at C-4,C-12 and C-16 of stearic acid, respectively. Spectra were obtained of the labelled membranes in the presence of phenylethylamine (PE), dopamine (DA) and PE+DA, respectively, over a temperature range of 37° to -28°C using a Bruker 9.3 GHz spectrometer. The temperature dependence of the outer hyperfine splitting, A max, was unchanged by PE, DA and PE+DA with the spin labels in position C-4 and C-12 of the stearic acid in the synaptosomal membrane. The acyl chain segmental motion of the C-16 stearic acid spin label was slightly increased (decreased A max) by PE and DA respectively, but markedly enhanced with PE+DA over the temperature range 30° to -28°C. The order parameter, S, paralleling results of A max, reflected higher state of disorganization (greater fluidity) at 20Å in the membrane. Similarly, PE didn't alter the rotational motion of the long axis of the lipids (correlation time,τ) of the control membranes over the entire temperature range, while DA slightly decreased τ (12%) only from temperatures below -10°C. In the presence of PE, the acyl chain wobbling induced by DA was markedly potentiated (53%) throughout the temperature range 37° to -28°C.

These ESR results are similar to the electrophysiological data of Jones & Boulton (1980) in which iontophoretic injection of PEA produced no change in neuronal firing rate, but potentiated the time course of the action potential induced by DA. This ESR study affords biophysical confirmation for a neuromodulatory role of PEA, and possibly other trace amines.

Jones, R. S. and Boulton, A. A., Can. J. Physiol. Pharmacol. 50, 222-227 (1980).

TU-AM-B2 MOSSBAUER AND EPR SPECTROSCOPY ON SOYBEAN LIPOXYGENASE. W.R. Dunham, R.H. Sands, J.F. Thompson, R.T. Carroll and M.O. Funk, Biophysics Research Division, The University of Michigan, Ann Arbor, MI, 48109; US Plant Soil and Nutrition Laboratory, ARS-USDA, Ithaca, NY; Department of Chemistry, University of Toledo, Toledo, OH.

We have performed spectroscopic studies on samples of soybean lipoxygenase, prepared both from seeds and from cell cultures enriched in ^{57}Fe: Mossbauer spectroscopy on ^{57}Fe-enriched and natural abundance samples and low temperature EPR spectroscopy experiments, which included experiments on the Mossbauer samples. For the reduced state of the enzyme, the iron is high-spin ferrous (δ/Fe = 1.23 mm/s, QS = 3.26 mm/s, at T = 125°K). These parameters can be matched in the literature to iron compounds with octahedral oxygen environments. Upon oxidation with product, lipoxygenase gives a very wide pattern characteristic of S = 5/2 states, which is not significantly broadened by spin lattice relaxation at temperatures below 175K. Similar properties were also found in ferric diethylenetriaminepentaacetate (DTPA) samples, but not in ferric ethylenediaminetetraacetate (EDTA) samples. Because iron DTPA shares other chemical similarities to lipoxygenase (both reduced lipoxygenase and ferrous DTPA are stable to air) and because these properties are relatively rare for mononuclear, non-heme iron centers we are currently investigating iron DTPA as a model for the iron site in lipoxygenase.

TU-AM-B3 **OXYGEN EFFECTS ON THE METABOLISM OF NITROXIDES IN CELLS**

Kai Chen, Philip D. Morse, II, and Harold M. Swartz
University of Illinois College of Medicine and Illinois ESR Research Center, Urbana, IL 61801

The uses of nitroxides in complex biological systems to study membrane dynamics and as contrast agents for *in vivo* NMR or for ESR imaging has led to a need to understand thoroughly the reduction and reoxidation of nitroxides in cells. The products of the reduction of nitroxides in cells are the corresponding hydroxylamines. which cell can reoxidize back to the nitroxides in the presence of oxygen. The reduction and reoxidation of nitroxides in cells can be largely inactivated by heating to 70 °C or by treatment with trichloroacetic acid, or can be inhibited by some metabolic inhibitors. These data indicate that both the reduction and reoxidation of nitroxides are enzymatic or enzyme-mediated processes. The reduction of nitroxides occurs in the cytoplasm or near membrane surfaces, whereas reoxidation occurs within the membrane. Lipid soluble hydroxylamines are oxidized in living cells but their aqueous soluble analogs are not except for slow autoxidation of some pyrrolidine hydroxylamines. Reoxidation of lipid soluble nitroxides located at different positions within the membrane are all pseudo first order with respect to nitroxides which is consistent with reoxidation occurring in the membrane. For the lipid soluble nitroxides, the rate of reduction and reoxidation is very sensitive to oxygen and has different oxygen dependencies. The rate of reduction is a sharp function of intracellular oxygen concentration. Only hypoxic cells reduce nitroxides rapidly. The rate of reoxidation is proportional to the intracellular oxygen concentration. With addition of cyanide or azide, oxygen-dependent reduction of lipid soluble nitroxides in cells disappears, and oxidation of hydroxylamines is inhibited. SKF-525A, an inhibitor of cytochrome P-450, does not affect the oxygen dependence of the reduction and reoxidation of nitroxides in cells.

Supported by NIH grants RR 01811, GM 35534, and GM 34250.

TU-AM-B4 THE USE OF ^{13}C-NMR TO STUDY RESPIRATORY CONTROL IN THE ISOLATED PERFUSED RAT HEART. Steven D. Buchthal and Truman R. Brown, Fox Chase Cancer Center, Phila. PA 19117

The study of the mechanism of respiratory control in the intact heart has been limited by the inability to measure the different mechanical, metabolic and electrochemical variables simultaneously. These include energy demand (as measured by mechanical work), the levels of high energy phosphates, the pH gradient across the mitochondrial membrane and the redox potential. We report the identification of a resonance in the ^{13}C-NMR spectrum of perfused hearts from rats fed a niacin-free diet supplemented with 2-[^{13}C]-nicotinic acid in their drinking water as NAD. The concentration of NAD, as measured by the ratio of the peak area to that of 1-[^{13}C]-glucose from a capillary tube inside the perfusion chamber is 2.5 mM. The ^{13}C-NMR spectrum and a spectrophotometric assay of the acid extract from the same heart showed a similar concentration compared to the intact heart. We are currently building a double tuned coil to observe the ^{13}C and ^{31}P-NMR specra of the same heart. This will allow concurrent measurements of the metabolic and the electrochemical parameters involved in respiration and will lead to a better understanding of its control.

This work was supported by the SE Pennsylvania Chapter of the American Heart Association and by NIH (RR02231)-USDOE/OHER Stable Isotope Program at Los Alamos.

TU-AM-B5 SATURATION TRANSFER MEASUREMENTS OF CREATINE KINASE REACTION VELOCITY IN HUMAN SKELETAL MUSCLE. Lizann Bolinger, Sarah Englander, Glenn Walter, John Leigh and Joanne Ingwall, Metabolic NMR Research Resource, Univ of Pennsylvania, Philadelphia, PA and NMR Laboratory, Harvard Medical School, Boston, MA

Animal studies using ^{31}P-NMR saturation transfer to measure the velocity of the creatine kinase (CK) reaction (CrP + ADP $\xrightarrow{k_{for}}$ ATP + Cr, where CrP = creatine phosphate) in heart, brain and skeletal muscle in situ and ex vivo have shown that reaction velocity changes with enzyme and substrate concentration. The goals of this study were to develop methodology to measure CK reaction velocity in human skeletal muscle and to define the enzymology of the CK reaction at different workloads when [ADP] is expected to change. Here we report preliminary results obtained from a healthy, 20-year-old male. ^{31}P-NMR saturation transfer measurements were made at 1.83 Tesla using an one-turn 11.5 cm surface coil placed on the gastrocnemius muscle at rest and under tension caused by moving a 32, 41 or 54 kg weight by plantar flexion. Consistent with increased work, CrP/ATP decreased. Using literature values for [ATP=9.2mM], [total Cr=55 mM], Vmax (224 mM/s), K_{eq} (147, pH 7.06) and dissociation constants for MM-CK, we calculated [ADP] (μM); pseudo-first order rate constant, k (s^{-1}); measured and predicted from rate the equation reaction velocities (mM s^{-1}):

tension	CrP/ATP	[ADP]	k_{for}	v_{meas}	v_{pred}
rest #1	2.90	66	0.31	8.3	20
32 kg	2.56	83	0.47	11.0	21
rest #2	2.87	67	0.27	7.2	20
41 kg	2.17	109	0.49	9.8	22
54 kg	1.36	211	1.02	12.8	23

These results show that both [ADP] and pseudo-first order rate constant increases with work; however, since [CrP] decreases, both measured and predicted reaction velocities remain unchanged. The apparent Km for ADP for the reaction is 186mM, suggesting that [ADP] regulates the reaction in vivo.

TU-AM-B6 METABOLISM OF D-GLUCOSE IN A WALL-LESS MUTANT OF NEUROSPORA CRASSA EXAMINED BY ^{13}C NMR: EFFECTS OF INSULIN by N.J. Greenfield*, M.A. McKenzie*, F. Adebodun#, F. Jordan# and J. Lenard*. *Department of Physiology and Biophysics, UMDNJ-Robert Wood Johnson Medical School, Piscataway, N.J. 08854-5635 and the #Department of Chemistry, Rutgers University, Newark, N.J. 07102

^{13}C NMR has been used to investigate the metabolism of glucose by a wall-less strain of N. crassa. Using [1-^{13}C] or [6-^{13}C] D-glucose the major products identified in the ^{13}C NMR spectra were [2-^{13}C] ethanol, [3-^{13}C] alanine and C_1 and C_6 labeled trehalose. In addition there were smaller peaks corresponding to mannitol, labeled in the C_1 and C_6 position and [1-^{13}C] ethanol. Several observations suggested the existence of a substantial hexose monophosphate shunt: (1) a 70% greater yield of ethanol from C_6 than from C_1 labeled glucose; (2) C_1 labeled glucose yielded 19% C_6 labeled trehalose, while C_6 labeled glucose yielded only 4% C_1 labeled trehalose; (3) a substantial transfer of ^{13}C from C_6 labeled glucose to the C_3 position of alanine. Addition of insulin (100 nM) with the glucose had the following effects: (1) a 24% increase ($p<0.01$) in the rate of ethanol production and a 38% increase ($p<0.05$) in the rate of alanine production from [1-^{13}C] D-glucose; (2) a 35% increase in the yield of mannitol ($p<0.05$) from D-glucose; (3) an increase in the degree of randomization of label from the C_2 to the C_1 position of ethanol from 2.1% to 4.2% ($p<0.05$). Insulin thus appears to stimulate glycolysis in these cells in addition to increasing the production of CO_2 and glycogen as previously demonstrated.

TU-AM-B7 PHOSPHOLIPID ORDER AND DYNAMICS IN AN AMPHIPHILIC PEPTIDE-PHOSPHOLIPID MODEL MEMBRANE: A DEUTERIUM NMR STUDY. (Prosser, S.; Davis, J.; Department of Physics, University of Guelph, Guelph, Ontario, N1G 2W1.)

A unique model membrane system composed of a synthetic amphiphilic peptide (lys_2-Leu_{16}-Lys_2-Ala-amide) and a specifically labeled phospholipid (7,7-$^2H_2$-1,1,-dipalmitoyl-sn-glycero-3-phosphocholine) has been studied by ^2H NMR. The structure and organization of the peptide in the bilayer, in addition to the phase boundaries of the fluid and gel phases, have been determined previously (Biochem. 1983, 22, 5298, Biochem. 1985, 24, 1377, Biochem. 1985, 24, 5396). The system was studied from -20°C to 60°C, at molar peptide concentrations of 0%, 2%, 4% and 0%. By employing three multipulse sequences (Inversion Recovery, Quadrupolar Echo, and Jeener-Broeckart), spectra and relaxation times were obtained, from which segmental order parameters and the spectral density functions $J_0(0)$, $J_1(\omega_0)$,$J_2(2\omega_0)$,(ω_0=2πx56MHz) were determined. The consistency of these results with various motional models, and predictions for protein-lipid interactions, is discussed.

TU-AM-B8 EFFECT OF MALIGNANCY ON BLOOD PLASMA LIPOPROTEINS BY ^{13}C and ^1H NMR SPECTROSCOPY. G.D. Williams[1], D.E. Cunningham[1], K.R. Metz[2] and I.N. Gorman[1]. [1]Department of Radiology, The Pennsylvania State University College of Medicine, Hershey, PA 17033 and [2]Harvard Medical School, Boston, MA 02215.

It has been reported that the proton NMR linewidth of lipoprotein aliphatic lipid resonances of plasma correlates well with the presence or absence of malignant tumors in patients (1). Lipoprotein complexes have been shown to have characteristics similar to plasma membranes, and the NMR spectra are dominated by lipid resonances (2-3). In this study, we have sought a biophysical basis for the observed differences by employing natural abundance ^{13}C NMR relaxation measurements at 100 MHz. ^{13}C NMR dynamic studies can provide information on molecular motions and interactions at the segmental level (4). ^1H NMR lineshape and spin-lattice relaxation time (T_1) analysis have clearly demonstrated the multicomponent nature of the lipid methylene and methyl resonances. For the case of untreated malignancy, there appears to be a significant increase in the mobile triglycerides from VLDL or chylomicrons, resulting in an apparent narrowing of the composite NMR signal. Variations in the degree of unsaturation, cholesterol and phospholipid levels were measured from the high resolution ^{13}C spectra. The importance of careful spectroscopy, lipoprotein stability, sample temperature and thorough patient records will be discussed. (1) Fossel, E.T. et al., N. Engl. J. Med., 315, 1369 (1986). (2) Wright, L.C. et al., FEBS LETT, 203, 164 (1986). (3) Hamilton, J.A. and Morrisett, J.D., Methods Enzymol., 128, 472 (1986). (4) Brown, M.F. and Williams, G.D., J. Biochem. Biophys. Methods, 11, 71 (1985).

TU-AM-B9 ^{19}F NMR DETECTION OF THE EFFECTS OF LEAD TOXICITY ON INTRACELLULAR [Ca^{2+}] IN OSTEOBLASTIC BONE CELLS. Dowd, T.L., Schanne, F.A.X., Gupta, R.K., and Rosen, J.F. Albert Einstein College of Medicine, New York, NY 10461.

The molecular basis of lead toxicity at the cellular level is largely unknown. Bone is the major reservoir of body lead. We measured the effect of lead on calcium homeostasis in bone cells. Intracellular [Ca^{2+}] was determined using the fluorinated intracellular chelator 5FBAPTA (1,2-bis-2-amino-5-fluorophenoxyethane-N,N,N',N'-tetraacetic acid) which allowed simultaneous observation and quantitation of two distinct resonances for chelated intracellular Ca^{2+} and Pb^{2+}. A rat osteoblastic cell line, ROS 17/2.8, attached to collagen coated microcarrier beads suspended in F12 medium was preloaded with 20 uM acetoxymethyl ester of 5FBAPTA for 0.5 h at 37° C. The cell suspension in a 10 mm NMR tube was continuously perfused with oxygenated (95% O_2 + 5% CO_2) medium in the NMR spectrometer. The K_d for Ca-5FBAPTA was determined in solutions that mimicked intracellular ionic conditions (0.5 mM $MgCl_2$, pH 7.1, 30° C). A Scatchard analysis using a Ca^{2+} ion selective electrode as well as an NMR determination gave an average K_d of 451 ± 37 nM (S.E.). Intracellular [Mg^{2+}] and pH were determined from the ^{31}P NMR spectrum of the osteoblasts. The results indicate that the basal intracellular [Ca^{2+}] of the ROS bone cell line is 175 ± 17 nM. Treatment with parathyroid horomone at 400 ng/ml induced a 30% increase in intracellular free Ca^{2+}. The addition of 25 uM Pb^{2+} gave rise to a 25-100% increase in free Ca^{2+} about 2 h after addition. The appearance of an intracellular Pb-5FBAPTA resonance followed the increase in intracellular free Ca^{2+}. Our results support the hypothesis that perturbations in cellular Ca^{2+} homeostasis is an early expression of lead toxicity. (Supported by NIH Grants).

TU-AM-B10 **SOLUTION STRUCTURE REFINEMENT USING COMPLETE RELAXATION MATRIX ANALYSIS OF 2D NOE EXPERIMENTS: DNA FRAGMENTS.** Thomas L. James and Brandan Borgias, Departments of Pharmaceutical Chemistry and Radiology, University of California, San Francisco, CA 94143.

Two-dimensional NMR has considerable promise for detailed structural characterization of moderate size molecules (≤15000 daltons) in non-crystalline environments. The two-dimensional nuclear Overhauser effect (2D NOE) experiment, in particular, has the potential for yielding a large number of internuclear distances which may be used with other structural constraints to give a detailed molecular structure. We have examined the assumption of isolated spin pairs commonly used for analysis of NOEs and consequent errors in distance determinations. Consequently, we prefer to use the complete relaxation matrix analysis program (CORMA) we have been developing for 2D NOE spectra. In contrast to the approximate approach, exact intensities in the 2D NOE spectrum are calculated for a given three-dimensional array of protons after diagonalizing the relaxation matrix. We have used CORMA to determine structures quantitatively in small molecules, but our primary interest is in biopolymers. Experimental 2D NOE spectra obtained at a series of mixing times have been compared with CORMA-generated theoretical spectra for structural models based on either x-ray diffraction-derived molecular coordinates or coordinates derived from molecular energy refinement calculations. As intensities in 2D NOE spectra are quite sensitive to internuclear distances, comparison of theoretical and experimental spectra has in some cases provided insights into details of sequence-dependent DNA duplex structure. More recently, we have begun developing a program for *refinement* of structures of modest-sized biopolymers by minimizing the error between the calculated and experimental 2D NOE spectra. We investigated the consequences of experimental errors in peak intensities on the refinement process for nucleic acid structure. To date, major conclusions are: (a) Known structural constraints in the molecular framework are necessary for successful refinement of the structure when realistic errors are encountered in the data. (b) With the relatively large size of diagonal peaks, errors in diagonal peak intensities completely destroy the refinement if they are included in calculation of the residuals. If diagonal peaks are ignored, the refinement is successful. (c) Spectral densities can be refined.

TU-AM-B11 **SOLID-STATE NMR OF CISPLATIN AND ANALOGS** **Rodolfo A. Santos, Wei-Jyun Chien, Gerard S. Harbison,** Department of Chemistry, State University of New York, Stony Brook, NY 11794; **James D. McCurry, James E. Roberts,** Department of Chemistry, Lehigh University, Bethlehem, PA 18015.

Using magic-angle spinning (MAS), we have obtained for the first time the ^{15}N chemical shielding tensors of the anti-cancer drug *cis*-diamminedichloroplatinum-II, and several of its analogs. Slow MAS spectra of ^{15}N labelled *cis*-diammineplatinum-II compounds reveal sideband patterns for the primary ^{15}N resonance and also for its ^{195}Pt satellites. These sideband patterns derive from the anisotropic NMR interactions in the material. From the sideband intensities of the primary resonance we obtain the principal values of the ^{15}N chemical shielding tensor; from those of the satellites we obtain the principal values of the convolved chemical shielding, dipolar and J tensors. Deconvolution of the tensors then gives the chemical shielding principal axis directions relative to the Pt–N bond. For our best-characterised system, the dithiocyanato- analog of cisplatin, we obtain two distinct ^{15}N shielding tensors, for the two crystallographically-distinct nitrogens in the molecule; the shielding tensor principal values (σ_{zz}, σ_{yy}, σ_{zz}) are (–77, –27, 5) and (–103, –32, –3) ppm, relative to 5.6N aqueous NH_4Cl. These shielding tensors are much more anisotropic than any previously obtained for an $-NH_3$ group; the anisotropy is due largely to the upfield shifted principal value σ_{zz}, which is found to be perpendicular to the Pt–N bond axis; while the downfield principal axis, whose shift is very similar to those usually obtained for $-NH_3$ groups, is oriented parallel to the Pt–N axis. This upfield shift is ascribed to the relativistic heavy-atom effect, previously observed in solution NMR of these compounds; the directionality of the shift confirms theoretical predictions. Results for other *cis*-diammineplatinum-II compounds are qualitatively similar, but the shielding anisotropies span a wide range, as would be expected from the wide range of isotropic ^{15}N chemical shifts observed. Large J-anisotropies (600 – 700 Hz) are also detected for the Pt–N interaction. The size of the shielding anisotropies suggests that solid-state ^{15}N NMR may be a valuable tool for obtaining structural information for the cis-platin complex with DNA.

TU-AM-B12 ^{19}F NMR IMAGING OF HALOTHANE DISTRIBUTION IN THE BRAIN.
C.B Conboy and A. M. Wyrwicz, Department of Chemistry, University of Illinois at Chicago, Chicago, Illinois 60680

Understanding the mechanisms of general anesthesia requires knowledge of the spatial distribution of anesthetic agent throughout the neuro tissue. We have applied ^{19}F NMR imaging to map the distribution of the fluorinated anesthetic, halothane, in the brain of a rabbit. The imaging of such an exogenous compound is hampered both by a short T_2 value and a low concentration. To alleviate the short T_2 problem we have combined the principle of volume selective excitation with a spin-echo imaging sequence to remove the gradient slice selection from the experimental echo time, TE. This approach allows for a minimum TE of 3.2 msec. There is a restriction on the minimum slice thickness obtainable and on the digital resolution. However, these limitations are not severe for imaging of nuclei of low concentrations. The imaging sequence we have developed contains a non-selective 180° pulse following the volume selective 90° pulse. Difficulties in image quality will arise due to inhomogenity of the B_1 field over the image volume. We have compensated for this by using a solenoid imaging coil which possess excellent B_1 homogeneity and allows for maximum sensitivity. We have also employed a multi-echo sequence in conjunction with the short TE spin-echo imaging sequence to eliminate the longer T_2 components from the resulting image. (Supported by UPHS grants GM29520, GM33415 and RCDA K04GM00503 to AMW).

TU-AM-C1 DEUTERIUM NMR STUDIES OF THE INTERACTION BETWEEN WATER AND NUCLEIC ACIDS. Rolf Brandes, David R. Kearns, and Allan Rupprecht,* Department of Chemistry, University of California, San Diego, La Jolla, CA 92093-0314, *Arrhenius Laboratory, Division of Physical Chemistry, University of Stockholm, Stockholm, Sweden

Solid samples of uniaxially oriented Li- and Na-DNA were hydrated with D_2O, and high resolution ^2H NMR was used to obtain lineshapes of the hydration water as a function of hydration level. It was found that the lineshape, and therefore the interactions, are different in Li- and Na-DNA. In Li-DNA, which remains in a B-type conformation throughout the hydration range studied, we observe the following. At low levels of hydration (0-4 D_2O/nucleotide) the ^2H spectra shows a single line, characteristic of isotropic averaging. At ~5 or more D_2O/nucleotide, the spectra suddenly exhibits a large doublet splitting, characteristic for anisotropic systems. The general trend is a decrease of this doublet splitting with increasing hydration. On the other hand, Na-DNA which remains in the A-form at low hydration levels, exhibits no splitting below a hydration of 10 D_2O/nucleotide. Between 10-20 D_2O/nucleotide, the splitting increases with increasing hydration. We discuss the interaction of water with DNA as a function of hydration within a conformational type, as well as the effect of a conformational change on the lineshapes.

TU-AM-C2 MULTINUCLEAR NMR STUDIES OF DNA AND DNA:LIGAND INTERACTIONS S. LAPLANTE, D. COWBURN*, J. ASHCROFT*, G. LEVY & P. BORER
BIOPHYSICS DEPT., BOWNE HALL, SYRACUSE UNIV., SYRACUSE, N.Y. 13244
& *ROCKEFELLER UNIV., 1230 YORK AVE., NEW YORK, N.Y. 10021-6399.

The non-exchangeable proton resonances of (1) [d(TAGCGCTA)]$_2$ were assigned by 2-D NOESY and COSY experiments. Three-dimensional structures in solution are being determined by a combination of ^1H NOESY experiments and complete relaxation matrix analysis. Carbon resonances of (1) and (2) [d(GGTATACC)]$_2$ have been assigned by direct comparison with monomers and chemical shift vs. temperature (δ vs. T) curves. Except for the 2′ and 5′ carbons, assignments have been made for the protonated carbon resonances of (1) by a proton-detected ^1H,^{13}C chemical shift correlation experiment. The base, 1′,(2′,2"),3′, 4′,(5′,5") correlations occur in separated regions of the 2D contour map. These ^{13}C assignments agree with those using the direct comparison method. Carbon δ vs. T curves show that about 25% of the base carbons exhibit deshielding trends upon duplex formation from single strands; these trends are probably due to H-bond (hydrogen bond) formation. Carbon nmr may be a useful tool in distinguishing H-bonding sites in DNA-ligand complexes. Netropsin was added (2) to explore the effects of H-bonding on the chemical shifts of the base carbons. Large deshielding was observed at carbon 4 of one adenine, thought to be involved in a strong H-bond from netropsin to AdoN3. Other changes in chemical shifts are consistent with disruption of a spine of hydration in the minor groove upon netropsin binding.

TU-AM-C3 INTERACTIONS OF POLYCYCLIC AROMATIC MUTAGENS WITH SUPERCOILED DNA INVESTIGATED BY KINETIC FLOW LINEAR DICHROISM TECHNIQUES. S.E. Carberry, N.E. Geacintov, and C.E. Swenberg*; New York University, Department of Chemistry, New York, NY 10003; * Armed Forces Radiobiology Research Institute, Bethesda, MD 20814.

Polycyclic aromatic hydrocarbons (PAH) are metabolized in living cells to potent mutagens and tumorigens which bind to cellular DNA. The formation and subsequent processing of such covalent adducts is believed to be a critical event in mutagenesis. The ultimate mutagenic metabolites of PAH compounds are the bay region diol epoxide derivatives. These compounds interact with DNA by forming first non-covalent complexes, followed by chemical reactions involving either the covalent binding of the PAH diol epoxide to DNA, or interactions with water to form the biologically inert tetraol hydrolysis products. We have developed kinetic flow linear dichroism techniques to study the unwinding and rewinding of supercoiled DNA induced by these PAH diol epoxides, some of which form intercalative non-covalent and covalent complexes, and some of which do not. The latter category includes 3-MCDE (3-methylcholanthrene diol epoxide); the (+) and (-) enantiomers of anti-BPDE (trans-7,8-dihydroxy-anti-9,10-epoxy-7,8,9,10-tetrahydrobenzo(a)pyrene) form intercalative non-covalent complexes, while the covalent adducts derived from the less mutagenic (in mammalian cells) (-) enantiomer also appears to be intercalative, and those derived from the highly tumorigenic (+) enantiomer are external in nature. The kinetics of these reactions can be monitored by following the unwinding and rewinding of supercoiled DNA accompanying these physical and chemical processes.

This work was supported in part by NIH Grant CA20851.

TU-AM-C4 **A MATHEMATICAL MODEL OF DNA SUPERCOILING** Robert K.Z. Tan and Stephen C. Harvey
Department of Biochemistry, University of Alabama at Birmingham, AL 35294

We present the results of a modeling study of supercoiled DNA. The DNA is modeled as a sum of quadratic functions of the deviation of the helicoidal parameters from the values for a linear DNA. The potential energy is the sum of terms for each base-pairs which for the i-th base-pair is:

$$E_i = k\alpha(\alpha-\alpha_0)_i^2 + k\beta(\beta-\beta_0)_i^2 + k\gamma(\gamma-\gamma_0)_i^2 + k\delta(\delta-\delta_0)_i^2$$

where α, β, γ and δ denote the helical twist, base-pair roll, base-pair tilt and the distance between adjacent base-pairs respectively. The corresponding quantities α_0, β_0, γ_0 and δ_0 are the helical parameters for the linear DNA before closure. These are predicted from the sequence using the ApA Wedge model of Trifonov et al. The force constants $k\alpha$, $k\beta$, $k\gamma$ and $k\delta$ are estimated from experimental values for the torsional and longitudinal elastic moduli.

The potential energy is then minimized with respect to α, β, γ and δ for each base-pair. The lowest energy that the DNA can attain is when these quantities are equal to the corresponding quantities in the linear DNA. However, this is not possible in a closed chain. As a result the DNA twist and writhe to redistribute the energy.

Simulations for short homogeneous chains of 360-mers show that they are very flexible, i.e. there are many possible structures separated by low energy barriers. We have observed only the toroidal form so far in our simulations although the interwound form cannot be ruled out especially for larger heterogeneous chains.

TU-AM-C5 IS KINETOPLAST DNA BENT PERMANENTLY, OR IS IT HINGED?
Michael Hogan, Nada Canaan and Robert Austin
Depts of Molecular Biology and Physics, Princeton University, Princeton NJ 08544

It has been shown that, when phased with the helix repeat, multiple copies of an oligo-A segment will induce curvature into a DNA helix. Crothers and colleagues have proposed a model for this effect which suggests that curved kDNA segments of that kind are best described as a rigid molecule with approximately 20 deg of bending associated with each oligo-A element. In apparent aggrement with the model, electron microscopy of a highly bent 219 bp long fragment of C. fasciculata kinetoplast DNA has suggested that it folds upon itself to form a circle. We have used singlet depletion anisotropy decay, field induced birefringence decay, and gel electrophoresis to study the motional dynamics of that 219 bp kDNA DNA fragment, and as a control, a random sequence 209 bp DNA fragment derived from the urchin 5S gene. We find that as predicted, the physical properties of the kDNA fragment suggest that it is not a linear rod. However, the fragment does not display the overall rotational dynamics expected for a 219 bp circle. We also find that the kDNA fragment displays significant segmental flexibility and that near 37C, or in the presence of orienting electric field energies above 2KT, the kDNA fragment becomes nearly indistinguishable from its linear (5S) isomer. Based upon those effects, we suggest that the aberrant physical properties of kDNA may not be due to rigid curvature. Instead, it may be more appropriate to model kDNA as a series of directional hinges. In the context of that model, the directionality of bending and the apparent bending angle which have been deduced from steady state measurements are a measure of the r.m.s bending flexibility which occurs at each (hinge-like) oligo-A segment.

TU-AM-C6 THE MOLECULAR AND CRYSTAL STRUCTURE OF AN ALTERNATING SEQUENCE IN THE RIGHT-HANDED A-DNA CONFORMATION. M. Sundaralingam, S. Jain and G. Zon, Department of Biochemistry University of Wisconsin, Madison, WI 53706 and Applied Biosystems, Foster City, CA 94404

The self-complimentary octadeoxynucleotide GTGTACAC has been crystallized in the tetragonal space group $P4_32_12$ with unit cell constants a = b = 42.43, c = 24.76A. The structure has been determined and refined to an R-factor of 16% using oscillation film data out to a resolution of 2.5A. The structure turned out to be a right-handed duplex in the A-DNA family, rather than the expected Z-DNA for such an alternating sequence. The base-pair tilt angle(av. 9.76°) and displacement from helix axis(av. 3.48A) are significantly less than the corresponding values in A-DNA fibers(19° and 4.5A respectively). These values for our octamer are generally on the lower side when compared to the other known A-DNA oligonucleotide crystal structures. The refinement studies are showing that most of the water molecules are located in the major groove.

A-DNA has been repeatedly seen for sequences that do not possess an AA dinucleotide stretch. The available data seem to indicate that the AA dinucleotide and A-tracks induce the B-DNA and bend structures. It can therefore be envisaged that sequences lacking the AA dinucleotide may well adopt the A-DNA like structures even in genomic DNA.

Work supported by NIH grant GM-17378

TU-AM-C7 AN INVESTIGATION OF THE STRUCTURAL SPECIFICITY OF POLYAMINES IN LEFT-HANDED Z-DNA FORMATION WITH A MONOCLONAL ANTI-Z-DNA ANTIBODY. T.J. Thomas and R.P. Messner; Department of Medicine, University of Minnesota, Minneapolis, MN 55455.

We developed an enzyme immunoassay to study the B-DNA to Z-DNA transition of poly(dG-m^{5}dC)·poly(dG-m^{5}dC) using a monoclonal anti-Z-DNA antibody, Z22. The polynucleotide was incubated with various concentrations of putrescine, spermidine and spermine for 1 h at room temperature. The polynucleotide-polyamine complexes were applied to microtiter plates and treated with Z22, alkaline phosphatase conjugated immunoglobulins and the enzyme substrate. No binding of Z22 to the polynucleotide was observed at low concentrations of the polyamines. Z-22 bound strongly to the polynucleotide at high concentrations of polyamines. At intermediate concentrations, a smooth transition curve was obtained. The concentrations of polyamines at the midpoint of B-DNA to Z-DNA transition were 2.7 mM, 32 uM and 1.8 uM for putrescine, spermidine and spermine, respectively. These values were in excellent agreement with those determined by UV and CD spectroscopic methods.

Using the enzyme immunoassay, we also determined the efficacy of a series of spermidine homologs, $H_2N(CH_2)_3NH(CH_2)_nNH_2$ (where n=2 to 8) to induce the B-DNA to Z-DNA transition of poly(dG-m^{5}dC)·poly(dG-m^{5}dC). Our results showed that spermidine was the most effective trivalent polyamine to provoke the Z-DNA conformation. The midpoint concentration of the homologs increased as the number of methylene groups between the $-NH_2$ and -NH- groups was altered in relation to that of spermidine. These results provide strong evidence for structural specificity in polyamine-induced B-DNA to Z-DNA conformational transition. The results will be interpreted on the basis of molecular models for the interaction of polyamines with polynucleotides.

TU-AM-C8 A Z-TYPE DNA HELIX WITH WATSON-CRICK CHAIN DIRECTIONS. A. T. Ansevin and Amy H. Wang Graduate School of Biomedical Sciences, University of Texas Health Science Center, Houston, Texas 77225.

Major problems of steric hindrance exist along the transition path from B- to Z-DNA. Unless base pair hydrogen bonds are broken, for which evidence is lacking, the major obstacle appears to lie in the conversion of Watson-Crick chain directions in B-DNA to counter-Watson-Crick chain directions in Z-DNA. As an alternative, we suggest a new DNA structure [Z(WC)] having the same chain directions as B-DNA, a left handed helix with Z-type backbones, a (dGdC) repeat unit, 12 base pairs per turn, and a mean height of 3.67 Å/base pair. Because the Z(WC)-helix differs only subtly from the Z-helix, most physical tests would be unable to distinguish the two. However, a few differences can be predicted. For instance, the Z(WC) structure explains the relative instability of left handed sequences in which A substitutes for G in an alternating purine-pyrimidine sequence, the promotion of a left handed helical structure by the addition of organic solvents or hydrophobic cations to the medium, the extremely slow exchange of one of the hydrogen bonded hydrogens in Z-type DNA, and the existence of conditions in which the B⟷Z transition should occur with a half time of only seconds. All of these observations favor the assumption that transitions of polymeric DNA to a left handed helix are to a Z(WC)-type structure, while short oligomers crystallize in a slightly more stable helix of the conventional Z-type geometry. We postulate that in nature, the only kinetically accessible left handed structure is the Z(WC)-helix.

Supported by Robert A. Welch Foundation grant G 1009.

TU-AM-C9 SPECTROSCOPIC CHARACTERIZATIONS OF A SYNTHETIC DNA OLIGOMER CONTAINING A B-Z JUNCTION AT HIGH SALT. Richard D. Sheardy, Department of Chemistry, The Pennsylvania State University-Hazleton, Hazleton, PA 18201 and Stephen A. Winkle, Department of Chemistry, Rutgers, The State University of New Jersey, New Brunswick, NJ 08903

Previous CD and UV spectroscopic studies on the DNA 16-mer shown below indicate that this molecule assumes a right-handed conformation at low salt. As the salt concentration is increased, the "B-end" of the molecule retains the right-handed conformation, while the "Z-end" of the molecule undergoes a transition to the left-handed conformation. This necessitates the formation of a B-Z junction between the two conformations.

```
C*-G-C*-G-C*-G-C*-G-A-C-T-G-A-C-T-G
G-C*-G-C*-G-C*-G-C*-T-G-A-C-T-G-A-C
     "Z-end"              "B-end"
```

(C* = 5-me-C)

Both proton and phosphorous NMR studies have confirmed the above observations. Temperature dependent H-NMR spectra of both the exchangeable and non-exchangeable protons of the duplex at low salt indicates that the "B-end" of the molecule melts before the "Z-end". However, similar studies of the duplex at high salt indicate a conformational transition in the "Z-end" well below the melting temperature. Studies are currently being carried out to determine if the transition is a Z back to B transition, or if a "bubble" is forming at the junction.

TU-AM-C10 AN ALPHA-HELICAL PEPTIDE MODEL FOR NON-SPECIFIC PROTEIN-DNA INTERACTIONS.
Adam Zlotnick and Stephen L. Brenner, E. I. du Pont de Nemours and Co., Inc., Wilmington, DE 19898.

The sequence-independent binding of proteins to DNA involves electrostatic interactions with the DNA phosphate backbone and/or stacking interactions between aromatic amino acids and nucleic acid bases. Several proteins that bind to single-stranded DNA contain amino acid sequences predicted to form structurally similar motifs: alpha-helices in which amino acids are segregated by charge to opposite faces of the helix. We propose that the positively charged face of such helices interacts with the phosphate backbone of DNA, providing some or all of the binding free energy. The recA protein of *E. coli* provides one model system. It is known that protein-phosphate interactions are involved in recA-DNA binding and genetic evidence suggests that the DNA-binding domain is at the N-terminus of recA. At neutral pH, the N-terminal 23 amino acids of recA protein are predicted to be in an alpha-helical conformation and have a net charge of +2, with +5 charges on one face of the helix, -3 on the opposite face. We have synthesized a peptide based on the recA N-terminus, NH2-AIDENKQKALAAALGQIEKQFGKG-CONH2, and studied its binding to DNA. As determined by circular dichroism, the peptide helicity increases from ca. 0% to 40% upon addition of peptide to poly(dT) in water at 25 C. Both circular dichroism and fluorescence titrations using etheno-M13-DNA, yield a site size of 5 bases per peptide, as predicted by modeling. Binding is very salt-sensitive, consistent with an electrostatic interaction, and, surprisingly, exhibits positive cooperativity. The peptide binds to different DNA's with the same relative affinity as recA protein, i.e. poly(dT) > ethenoDNA > poly(dA) > dsDNA. This correlates with the relative difficulty in unstacking the bases to form an extended single-strand.

TU-AM-C11 DIRECT EVIDENCE FOR TWO ssDNA-BINDING SITES IN A RECA NUCLEOPROTEIN FILAMENT.
Richard S. Mitchell, Adam Zlotnick, and Stephen L. Brenner (Intro. by Mark L. Pearson),
E. I. du Pont de Nemours and Co., Inc., Wilmington, DE 19898.

Genetic recombination in *E. coli* is catalyzed by the recA gene product. The active quaternary structure is a helical recA protein filament containing ca. 6 protein monomers of 38 kDa per helical turn. The exchange of homologous DNA between DNA duplexes is initiated by recA protein binding to a single-stranded region of DNA, a search for homologous sequences, then an ATP-dependent exchange of DNA between the duplexes. The precise position of the DNA in the recA helix is not known, and reported site sizes for recA-ssDNA complexes vary from 3-7 bases/recA monomer. We have studied the binding of recA protein to ssDNA using (a) the fluorescence of etheno-M13-ssDNA as a monitor of DNA-binding, (b) the ssDNA-dependent recA ATPase. Measurements of ATPase and fluorescence were made on identical samples. The site size by ATPase assay is 3.0-3.5 bases/recA, while fluorescence yields values of 6-7 bases/recA. Titration measurements made by adding recA protein in small aliquots to DNA saturate at ca. 50% of the ATPase activity seen when recA and DNA are mixed directly at the highest recA concentration used in the titration. Measurements of the etheno-DNA fluorescence on the same samples, on the other-hand, give identical results independent of the method of recA protein addition. These results suggest a model in which (a) the recA protein helix has two ssDNA binding sites, (b) the ATPase of the helix is fully activated by binding one strand of ssDNA, (c) the fluorescence of etheno-DNA is enhanced when bound to either site, and (d) neither strand of DNA in the complex containing two strands is readily available to bind additional recA protein, even under ATPase conditions.

TU-AM-C12 THE HISTONE OCTAMER: A CONFORMATIONALLY FLEXIBLE STRUCTURE. G.D. FASMAN AND K. PARK, Department of Biochemistry, Brandeis University, Waltham, MA 02254

The literature contains conflicting data concerning the conformation of the histone octamer in both the crystal and in solution, as well as in the nucleosome. The conformation of the histone octamer complex has been shown herein, by circular dichroism (CD) studies, to be highly dependent on the nature and concentration of the salt milieu. Two different salts were used, NaCl and $(NH_4)_2SO_4$, to study the dependency of the conformation of the histone octamer on the salt concentration. With increasing concentrations of NaCl, the α-helical content of the octamer increased, with a concomitant decrease in the β-sheet content, through a wide range of the salt concentrations (0.2M to 4.0M). At 2.0M NaCl, the concentration at which Uberbacher, Harp, Wilkinson-Singley & Bunick [Science 232, 1247-1249 (1986)] used small-angle neutron scattering to study the octamer's size and shape, the analysis of the CD curve yielded 44% α-helix, 16% β-sheet and 40% random structure for the octamer. On the other hand, in a relatively narrow range of the concentration of $(NH_4)_2SO_4$, from 2.0M to 2.5M, there was a transition from α-helix to random coil with no significant change in β-sheet content. At 2.3M, $(NH_4)_2SO_4$, the concentration at which Burlingame, Love & Moudrianakis [Science 223, 413-414 (1984)] used to obtain histone octamer crystals, a higher α-helical content was found by CD. The analysis of this CD curve yielded a secondary structure with 49% α-helix and 51% β-sheet. Even though a direct comparison between the nucleosome core particle and histone octamer cannot be made, these results would indicate that the histone core and nucleosome can be viewed as very pliable structures, whose conformation can be altered by a change in local solvent milieu, partially resolving the contradictory claims concerning the X-ray analysis of crystals obtained under varying conditions.

TU-AM-C13 EFFECT OF STACKING INTERACTIONS WITH POLY (dT) ON THE TRIPLET STATE DECAY KINETICS OF TRPS 40 AND 54 OF E.COLI SINGLE STRANDED DNA BINDIDG PROTEIN (SSB). D. Tsao, J.R. Casas Finet, A. H. Maki, Department of Chemistry, University of California, Davis, CA 95616 & J.W. Chase Department of Molecular Biology, Albert Einstein College of Medicine, Bronx, NY 10461. (Introd. by Y. Yeh).

Optically detected magnetic resonance (ODMR) has been used to study the complex formed between a double point mutated SSB (Trp 88, 135→Phe) and poly (dT). From previous work[1] using single Trp→Phe point mutants we know that among the 4 Trps of SSB, only Trps 40 and 54 are involved in ss DNA binding via stacking interactions. Fluorescence titrations show that the double point mutated SSB binds poly (dT) as tightly as does native SSB. Selective excitation and emission wavelength detection was employed to measure the individual sublevel decay constants of Trps 40 and 54 in the double point mutated protein using zero field ODMR. Stacking of Trp 40 with thymine bases leads to a relatively small increase in the decay constants. We find k_x, k_y, k_z = 0.43, 0.070, 0.037 s^{-1}, respectively, which differ very little from unstacked Trp. For Trp 54, however, we find a large selective increase of k_x, which results from a unique interaction with poly (dT). For Trp 54, k_x, k_y, k_z = 1.13, 0.081, 0.055s^{-1}, respectively, in agreement with previous measurements[2] on single point mutated (Trp 88→Phe) SSB. These measurements demonstrate that although both Trp 40 and Trp 54 are involved in stacking interactions, these must be of a different type, since they lead to significant differences in triplet state kinetics. This research was supported in part by NIH Grants to AHM & JWC.

1. Khamis, M.I. et al., J. Biol. Chem., 262, 10938 (1987).
2. Zang, L.S. et al., Biophys. J., in press.

TU-AM-D1 MODIFICATION OF ARGININE RESIDUES IN THE Na,K-ATPase. Carlos H. Pedemonte and Jack H. Kaplan. Department of Physiology, University of Pennsylvania, Philadelphia, PA 19104.

α-Dicarbonyl reagents that react with arginine residues have been used to inhibit enzymes that have nucleotides as substrates. The characteristics of the inhibition which is protectable by the nucleotides suggest that the modified arginine is located at the substrate binding site. However the covalent reaction is not sufficiently stable under sequencing conditions to allow identification of the modified arginine. We hope to gain information about the structure of the Na,K-ATPase nucleotide binding domain by using p-azidophenylglyoxal (pAPG). pAPG is a heterobifunctional photoactivable cross-linking reagent with an α-dicarbonyl and an azido group which is highly reactive on UV irradiation. Treatment of purified Na,K-ATPase from dog kidney outer medulla with pAPG resulted in inhibition of the enzyme activity in a reaction that was first order with respect to time at different [pAPG]. The inhibition was unaffected by the presence of Na, K, Mg or Pi plus Mg but greatly reduced by ATP. After inhibition and removal of the excess pAPG the inactivation was stabilized by the presence of borate ions.The enzyme activity could be partially restored by incubation of the enzyme in Hepes-buffer in the absence of borate. This recovery of activity was abolished by irradiation of the enzyme suspension with 340 nm UV light,indicating that the reaction of the UV activated nitrene of pAPG stabilized the previous inhibition of the enzyme. None of the enzyme ligands affected either the recovery of the activity or the UV-dependent fixation of inhibition. SDS-PAGE of the pAPG-enzyme showed some changes in the pattern of fragmentation produced by trypsin in the low molecular weight range. This, and the fact that no change in the Rf of the enzyme subunits was observed, indicates that the cross-link produced by pAPG is an intramolecular one. Supported by NIH HL30315.

TU-AM-D2 THE MECHANISM OF ACTIVE ACCUMULATION OF CHLORIDE ACROSS THE MEMBRANE OF AMPHIBIAN DORSAL ROOT GANGLION NEURONES STUDIED WITH ION-SELECTIVE MICROELECTRODES. F.J. Alvarez-Leefmans, S.M. Gamiño+, F. Giraldez* and I. Noguerón. Dept. of Pharmacology, CINVESTAV-IPN, Apdo. Postal 14-740, México 07000, D.F.; +Dept. of Neurobiology, IMP, Calz. Xochimilco 101, México 14370, D.F. and *Dept. of Physiology, Fac. of Med. 47005 Valladolid, Spain.

The intracellular chloride activity (a^i_{Cl}) in the cell bodies of sensory neurones of frog dorsal root ganglia (DRG) is higher than predicted for a passive distribution (Alvarez-Leefmans et.al. Biophys. J. 49, 413a, 1986). This implies that Cl^- is actively accumulated across the membrane of these neurones. It also explains the depolarizing action of GABA on these cells. The aim of the present work was to further characterize the nature of this inwardly directed Cl^- transport. Em and a^i_{Cl} were measured simultaneously with double-barrelled Cl^- selective microelectrodes (LIX Corning 477913). In Ringer buffered with HEPES (5 mM) and equilibrated with air or 100% O_2, Em was -57.7± 1.0 mV and a^i_{Cl} was 23.6±1.0 mM (n=53). a^i_{Cl} was 2.6 times the expected for an equilibrium distribution. Removal of external Cl^- led to a reversible fall in a^i_{Cl}. Initial rates of decay and recovery of a^i_{Cl} were 4.1 and 3.3 mM min^{-1} respectively. During the recovery of a^i_{Cl} the movement of Cl^- occurred without changes in Em and against the driving force for a passive distribution. The steady-state a^i_{Cl} depended on the simultaneous presence of extracellular Na^+ and K^+. The active reaccumulation of Cl^- after intracellular Cl^- depletion was abolished in the absence of either external Na^+ or K^+. The reaccumulation of Cl^- was inhibited by furosemide ($0.5\text{-}1x10^{-3}$M) or bumetanide (10^{-5}M). It is suggested that a Na:K:Cl co-transport system mediates active transport of Cl^- across the membrane of DRG neurones. (Supported by CONACYT, Mexico).

TU-AM-D3 IDENTIFICATION OF A 200K DALTON COMPONENT OF THE Na,K,Cl-COTRANSPORT SYSTEM IN MEMBRANES FROM DOGFISH SHARK RECTAL GLAND. Bliss Forbush III and Mark Haas, with the technical assistance of John T. Barberia, Mt. Desert Is. Biol. Lab., Salsbury Cove ME, 04672; and Depts. of Physiology and Pathology, Yale University School of Medicine, New Haven, CT 06510.

We have previously found that radiolabeled loop diuretics bind to membranes from shark rectal gland (Biophys J, *37*, 161, 1982), dog kidney, and duck red cell, in a manner consistent with binding to inhibitory sites on the Na,K,Cl-cotransport system. Using [^{3}H]4-benzoyl-5-sulfamoyl-3-(3-thenyloxy) benzoic acid (BSTBA), a photosensitive loop diuretic, we have found that a 150K dalton peptide is photolabeled in dog kidney membranes (Am. J. Physiol., *253*, C243-C252, 1987) and duck red cells. Here we report photolabeling of the cotransport system in rectal gland membranes. A crude membrane fraction was prepared by differential centrifugation of homogenate of fresh rectal glands; the amount of saturable [^{3}H]BSTBA binding to these membranes was 20-80 pmol/mg protein. [^{3}H]BSTBA was bound by incubation of membranes for 20 min at 20 °C,and after removal of free [^{3}H]BSTBA by centrifugation, the resuspended sample was photolyzed for 20 min at 0°C. As shown here, when membrane proteins were separated by SDS gel electrophoresis, label was found to be incorporated in only one band at 200K daltons. Maximal incorporation represented about 10% of the reversibly bound diuretic, was dependent on the presence of Na, K, and Cl in the binding medium, and was blocked by unlabeled bumetanide. The 200K dalton peak of incorporation is broad, as are the 150K dalton peaks seen with kidney or red cell membranes, suggesting post-translational modification of the cotransport protein. It is hoped that the large amount of the cotransport protein in membranes from rectal glands (more than 10-fold the diuretic binding compared to kidney membranes) will facilitate its purification. (Supported by a Lucille P. Markey fellowship and NIH AM17433).

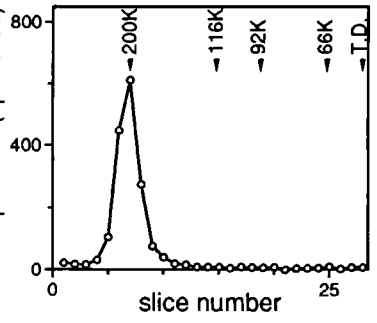

TU-AM-D4 FURTHER EVIDENCE AGAINST THE K^+-pNPPASE BEING A PARTIAL STEP IN THE REACTION SEQUENCE OF THE GASTRIC H^+,K^+-ATPase: EFFECTS OF CATIONS, ANIONS, NUCLEOTIDES, LOOP DIURETICS AND THE ENDOGENOUS ACTIVATOR. Tushar K. Ray and Pratap K. Das. Dept. of Surgery, SUNY Health Science Center, Syracuse, NY.

Several reports provided critical evidences suggesting the K^+-pNPPase associated with the gastric H^+,K^+-ATPase (Ray and Nandi Biochem. J. 233:231-238, 1986), and Na^+,K^+-ATPase (Nandi et al Fed. Proc.45:1905,1986) not to represent the partial step of the corresponding ATPase reactions. The present study provides further support for the said idea. Thus, low (50 μM) concentrations of Zn^{+2}, Hg^{+2} and Ca^{+2} exhibit inhibition of the K^+-pNPPase without affecting appreciably the H^+,K^+-ATPase activity while inhibiting simultaneously the H^+,K^+-ATPase mediated uptake of H^+ inside the gastric microsomal vesicles. Inorganic phosphate (1-5mM) also differentially inhibit the K^+-pNPPase without affecting appreciably the H^+,K^+-ATPase activity. Eventhough ATP inhibits the K^+-pNPPase and vice versa, other nucleotides such as ADP, CTP, and ITP (within 0.4mM) showed only differential inhibition of the K^+-pNPPase. Interesting differential effects of the loop diuretics were also observed. Thus, while furosemide and phloridzin inhibited the H^+,K^+-ATPase by competing with ATP, both agents appreciably (about 80%) stimulated the K^+-pNPPase activity. Stimulation of the latter reaction was blocked by DTT suggesting the involvement of some -SH groups. The data clearly argue against the K^+-pNPPase being a partial reaction of the H^+,K^+-ATPase.

TU-AM-D5 CALMODULIN BINDING AND ITS EFFECT ON Ca^{2+}-ATPase ACTIVITY IN TWO ENZYME FORMS. D. Kosk-Kosicka, and T. Bzdega, University of Maryland, School of Medicine, Baltimore, MD 21201.

The $C_{12}E_8$ solubilized Ca^{2+}-ATPase purified from human erythrocytes was studied to determine the mechanism of its activation by calmodulin. The dependence of Ca^{2+}-ATPase activity on the enzyme concentration showed a transformation from a calmodulin dependent to a calmodulin independent form with a $K_{1/2}$=11 nM and a Hill coefficient of nH=2.1. Consistent with this interpretation the inclusion of higher $C_{12}E_8$ concentrations progressively shifted the $K_{1/2}$ for this transformation to larger values. In all cases calmodulin decreased the $K_{1/2}$ ~1.8 fold without affecting the maximal velocity. This points to calmodulin facilitating interactions between enzyme molecules.

Activation of the Ca^{2+}-ATPase by calmodulin has revealed a 1:1 stoichiometry, with a K_d=1.6 nM. We have demonstrated by use of calmodulin-Sepharose chromatography that both, the calmodulin dependent and independent Ca^{2+}-ATPase forms, bind calmodulin even though stimulation of activity is seen only with the former one.

Our data suggest that the Ca^{2+}-ATPase undergoes a reversible oligomerization and that calmodulin increases the probability of this process. According to this hypothesis only oligomers are fully active.

TU-AM-D6 CURRENT-VOLTAGE RELATIONSHIP OF THE BACKWARD-RUNNING Na/K PUMP IN VOLTAGE-CLAMPED INTERNALLY-DIALYZED SQUID GIANT AXONS. R.F. Rakowski, Paul De Weer, and David C. Gadsby. Marine Biological Laboratory, Woods Hole, MA 02543.

To reverse the Na/K pump cycle and so generate inward pump current (PDW & RFR, *Nature* **309**:450-2, 1984), axons were bathed in 400 mM Na, 75 mM Ca, K-free seawater containing 200 nM TTX and 5 mM 3,4-diaminopyridine to diminish Na- and K-channel currents, and internally dialyzed with a Na-free, 120 mM KHEPES, 5 mM ADP, 5 mM P_i, and 25 mM L-arginine solution containing 50 µM atractyloside and 1.25 mM diadenosine pentaphosphate to suppress formation of ATP, and 25 mM phenylpropyl-triethylammonium-Br to further reduce K conductance; temperature, 17°C. Two ancillary voltage-clamp circuits held the central and end pools at the same voltage to prevent current flow between them and so eliminate electrical end effects. Na/K pump current was determined as the change in membrane current on sudden exposure to 100 µM dihydrodigitoxigenin (H_2DTG). From repeated exposures at different holding potentials (V_H), inward pump current was found to decline steadily with depolarization, from an apparent plateau level of -0.24±0.03 μAcm^{-2} (±SD, n=5, V_H -100 to -80 mV) to practically zero at +30 mV. In other experiments, the current-voltage relationship of the backward-running Na/K pump was determined as the difference between steady-state membrane current-voltage curves obtained using down-up-down staircases of 1-s voltage steps, from -110 to +30 mV, before and during exposure to 100 µM H_2DTG. The two methods yielded the same monotonic voltage dependence of inward pump current with no evidence of the region of negative slope conductance reported previously. Control measurements demonstrated that these new results could not be attributed to changes in residual K current. Absent a region of negative slope conductance, the Na/K pump reaction cycle is not required to include more than one voltage-dependent step.
Supported by NIH grants NS 22979(RFR), NS 11223(PDW), HL 36783 and the Irma T. Hirschl Trust(DCG).

TU-AM-D7 **K TRANSLOCATION BY THE Na/K PUMP IS VOLTAGE-INDEPENDENT BUT POSSIBLY RATE-LIMITING.**
Anthony Bahinski, Masakazu Nakao, and David C. Gadsby. *The Rockefeller University, New York, N.Y. 10021*

To examine voltage dependence of the Na/K pump cycle, pump current was determined as strophanthidin-sensitive (0.5-2 mM) current in guinea-pig ventricular cells voltage-clamped via wide-tipped pipettes. Solutions were designed to minimize channel and Na/Ca exchange currents but sustain four modes of Na/K pump activity. At 50 mM $[Na]_i$ and 150 mM $[Na]_o$, withdrawal of K_o interrupted Na/K transport and abolished steady pump current; but voltage steps elicited transient pump currents (abolished by oligomycin, and not seen in the absence of ATP or of Na_i and Na_o), demonstrating that Na translocation involves net charge displacement within the membrane field and is thus *voltage-dependent*. Addition of K_o activated steady, while diminishing transient, pump currents; yet, even at 5.4 mM $[K]_o$, small transients preceded new steady pump currents following voltage jumps. The pump cycle was reversed, generating steady inward current, by removing Na_i and K_o, setting $[K]_i$ and $[Na]_o$ at 150 mM, and adding ADP+P_i to the ATP in the pipette. Inward pump current increased as membrane potential was made more negative, from almost zero at +50 mV towards an apparent plateau level near -100 mV, and voltage steps still caused small transient pump currents to precede the new steady currents. Replacing all Na_o with N-methylglucamine and adding 5.4 mM $[K]_o$, while retaining the high [K], Na-free internal solution with ATP, ADP and P_i, limited the pump to K/K exchange; neither transient nor steady pump currents could then be seen, showing that K translocation does not involve net charge movement and is therefore *voltage-independent*. The monotonic voltage-dependence of inward and outward steady pump current implies net charge movement in only one direction in each pump cycle, consistent with it including a single voltage-dependent step (Na translocation). The transient currents reflect voltage-dependent redistribution of cycle reactants, indicating that the voltage-dependent step is relatively fast, i.e. that a voltage-insensitive step rate-limits the pump cycle. The $[K]_o$ sensitivity of outward pump current at positive potentials suggests that that voltage-independent rate-limiting step might be K translocation. Supported by NIH grants HL 14899 & HL 36783, the AHA NYC Affiliate, and the Irma T. Hirschl Trust.

TU-AM-D8 **VOLTAGE DEPENDENCE OF THE Ca_i-ACTIVATED Na_o-DEPENDENT CURRENT IN SQUID AXONS.** C. Caputo, F. Bezanilla and R. DiPolo. CBB IVIC, Apdo 21827, Caracas, 1020A & Dept. of Physiol., UCLA, Los Angeles, CA.

A $[Na]_o$-dependent $[Ca]_i$-activated membrane current can be measured in intracellularly dialyzed voltage clamped squid axons, in which most of the currents are abolished or reduced; the direction and magnitude of this current are determined by the Na and Ca gradients (DiPolo et al.1987. Biophys. J. 51:386a.). We have determined the current-voltage (I-V) relationship associated with the operation of this system using voltage clamp pulses in the range of -120 to +120 mV. The axons were bathed in a solution containing in mM: TEACl, 50; $CaCl_2$,10; $MgCl_2$, 50; NaCl, 200 to 0; NMG-Cl (N-methylglucamine), variable; TRIS-MOPS, 20; pH=7.8; TTX, 400nM. The dialysis solution contained, in mM: Na-aspartate, 0 to 200; NMG-aspartate, variable; TEA-aspartate,100; TRIS-EGTA, 1; $MgCl_2$, 2; TRIS-MOPS, 20; pH=7.3; osmolality = 1000 mOsm. $CaCl_2$ was added to set $[Ca]_i$ from 100 to 400 uM. The axons were clamped at their resting potential, between -11 and -4 mV, and the I-V relationships were obtained before, during and after dialyzing the axons with solutions free of ionic calcium. The current difference in the presence and absence of internal calcium was obtained for each voltage pulse, after subtraction of the Ca_i-activated steady current.

With 200 mM Na_o and 20 mM Na_i, the current showed more voltage dependence in the negative potential region and in two axons the current had a reversal potential (RP) of +71 and + 66 mV respectively, close to +79 mV which is the expected RP value for a 3Na-1Ca exchange system. Na and Ca gradients were changed to expected RP values of -4, +65 and +96 (2 cases) mV and the experimental values obtained were -8 +61 and +86 and +84 mV respectively. In addition, when the expected RP values were more negative than -120 mV or more positive than +120 mV the current was always outward or inward respectively. These results show that the measured Ca_i-activated sodium current has properties expected from a Na/Ca exchange mechanism with an stoichiometry of 3 Na to 1 Ca. Supported by MDA, USPHS grant GM 30376, and NSF-CONICITS1-1566.

TU-AM-D9 Na-Ca EXCHANGE BY TRANSVERSE TUBULE VESICLES ISOLATED FROM FROG SKELETAL MUSCLE.
Paulina Donoso and Cecilia Hidalgo*. Departament of Physiology & Biophysics, Faculty of Medicine, Universidad de Chile, and *Centro de Estudios Cientificos de Santiago, P.O. Box 16443, Santiago 9, Chile.

Transverse tubule (T-tubule) vesicles isolated from frog skeletal muscle display Na-Ca exchange activity, whereas T-tubule vesicles isolated from rabbit skeletal muscle do not. In contrast, surface membrane-enriched vesicular preparations isolated either from frog or rabbit muscle, both show significant levels of Na-Ca exchange activity. These findings indicate that while in rabbit skeletal muscle the exchanger is restricted to the surface membrane, in frog the exchanger is present in both membrane systems.

The Na-Ca exchange activity of T-tubule vesicles from frog muscle is electrogenic, as shown by the fact that the rates of Na-Ca exchange vary as a function of the membrane potential imposed across the T-tubule vesicles by potassium gradients in the presence of valinomycin. The Na-Ca exchanger operates both in the forward and in the reverse mode; the K_m values for calcium and sodium in the forward mode are 3-5 uM and 70 mM, respectively. The rates of exchange increase upon increasing pH from 7 to 9, and are drastically decreased by amiloride. In the absence of sodium, the exchanger carries out Ca-Ca exchange. The rates of Ca-Ca exchange are stimulated by potassium in the intravesicular side. The K_m value for calcium of the Ca-Ca exchange reaction is 6 uM, in the same range as the K_m value for calcium of the Na-Ca exchange reaction.
Supported by NIH grants HL 23007 and GM 35981, MDA, FONDECYT # 1340, DIB # 2149 from Universidad de Chile, and by the Tinker Foundation.

TU-AM-D10 DIGITAL IMAGE ANALYSIS OF 2-D Na,K-ATPase CRYSTALS: DISSIMILARITY BETWEEN PUMP UNITS. H.C. Beall, D.F. Hastings, and H.P. Ting-Beall. Department of Anatomy, Duke University Medical Center, Durham, NC 27710.

Two-dimensional crystals of purified Na,K-ATPase were induced by treatment with phospholipase-A_2 and vanadate. The negatively stained crystals were imaged by electron microscopy and analyzed by digital image processing. Two dimensional averaged projections of the crystals were calculated by the technique of correlation analysis, utilizing SPIDER (System for Processing of Image Data in Electron microscopy and Related fields) image processing software. The signal-to-noise ratio of the scanned micrographs was 0.3:1, and the limiting resolution of the correlation averaging procedure was 1.8 nm. The calculated dimensions of the unit cell were found to be 13.3 nm x 4.59 nm with included angle of 98 degrees, comparable to those reported by others. However, the two protomers of the unit cell were found always to be dissimilar in shape and in orientation. All protomers on one side of the dimer ribbon had a triangular outline and all protomers on the opposing side had a comma shape. This dissimilarity could be explained by two slightly different orientations of identical protomers: one orientation for all protomers on one side of the dimer ribbon, and another orientation for all protomers on the opposing side of the ribbon. An alternative explanation is that the dimers are formed from two dissimilar protomers: the dimers form into ribbons that have all the protomers on one side with one conformation while all protomers on the opposing side of the ribbon have a different conformation. This dissimilarity supports the concept, already raised by other researchers, that native membranes contain two slightly different forms of Na,K-ATPase. (Work supported by NIH grants GM27804 and S10-RR02283, and NSF grant NSF-PCM-8306638.)

TU-AM-D11 FLUORESCENCE ENERGY TRANSFER DETECTS DISTANCE CHANGES ACCOMPANYING PHOSPHORYLATION OF THE CA-ATPASE OF SARCOPLASMIC RETICULUM. D.J. Bigelow, T.C. Squier, and G. Inesi, Dept. of Biol. Chem., Univ. of Maryland School of Medicine, Baltimore, MD 21201.

We have measured resonance energy transfer between two donor-acceptor pairs localized on different domains of the Ca-ATPase of sarcoplasmic reticulum in order to determine whether changes in tertiary structure accompany active calcium transport. Energy transfer was determined from both steady-state intensities and time-resolved lifetimes of IAEDANS, specifically bound to two proximal cysteines on the B tryptic fragment, using two acceptors: (1) FITC, covalently bound at the nucleotide site, also on the B fragment, and (2) 4-dimethylaminophenylazophenyl-4'-maleimide (DABMI), bound on the A_1 subfragment. Neither binding of calcium to the high affinity sites nor phosphorylation by inorganic phosphate is accompanied by detectable changes in the distance between IAEDANS and FITC, suggesting that the B fragment does not undergo any large-scale (>1 A) physical distortion under these conditions. On the other hand, measurements of energy transfer from IAEDANS to the acceptor DABMI, on the A_1 subfragment, demonstrate that phosphorylation with inorganic phosphate or addition of μM VO_4 results in a 4 ± 1 % increase in energy transfer, that is reversible with subsequent addition of calcium. Addition of calcium to the nonphosphorylated enzyme results in no change in energy transfer. Our observations suggest that coincident with phosphorylation by P_i that either the A and B domains move with respect to one another or that there is a change in the degree of interaction between Ca-ATPase polypeptide chains.

TU-AM-D12 REVERSIBLE OXIDATIVE STIMULATION BY DIAMIDE OF OUABAIN-RESISTANT K:Cl TRANSPORT IN SHEEP RED BLOOD CELLS. P. K. Lauf, Dept.Physiol.& Biophys. Wright State Univ. Dayton,OH 45435.

Ouabain-resistant (OR) Cl-dependent K transport (K:Cl transport) in sheep red cells is activated by 1) cell swelling (Dunham & Ellory,J. Physiol.318:511,1981), 2) thiol (SH) group alkylation by N-ethylmaleimide (NEM) (Lauf & Theg, Biochem.Biophys.Res. Commun. 92:1422,1980), and 3) by removal of cellular bivalent ions through A23187 (Lauf, Am.J. Physiol. 249:C271,1985). A model has been proposed that all three interventions activate the same K:Cl transport pathway present in red cell membranes of sheep and other species (Lauf, J. Memb.Bio. 88:1,1985). We now report that K:Cl transport may be also activated by oxidation using the well known glutathione (GSH) oxidant, diamide. K:Cl transport was stimulated by diamide in a dose-dependent manner after more than 80% of cellular GSH was oxidized to its disulfide, GSSG. No effect of diamide was seen on OR Na fluxes. The action of diamide was fully reversed upon metabolic reconstitution with a ratio of 0.5 for the fractional restitution of K:Cl transport versus that of GSH suggesting that more than one molecule GSH is required to reverse the oxidative effect of diamide. The oxidative stimulation of K:Cl flux by diamide was also fully reversed by dithiothreitol with Hill coefficients of greater than unity suggesting chemical reduction of at least one if not two disulfide bonds. The action of diamide appears to be via SH groups which also react with monofunctional reagents such as NEM and iodoacetamide, and the oxidant methyl-methane-thiosulfonate. It is suggested that the K:Cl transport stimulation by diamide involves reversible oxidation of more than one SH group to mixed disulfides with other SH donating compounds present in the erythrocyte. This effect was most pronounced in low K and much less in high K sheep red cells consistent with the known genetic differences in the OR K fluxes of these cells. (Supp by NIH grant DK 37160).

TU-AM-E1 SINGLE NA CHANNEL CURRENTS FROM SQUID GIANT AXON FOLLOWING REMOVAL OF FAST INACTIVATION BY PRONASE. R.A. Levis, Dept. of Physiology, Rush Medical Center, Chicago, IL 60612

The patch voltage clamp was used to record single sodium channels from the internal surface of the cut-open squid giant axon. Axons were cut open in 0 K artificial sea water. After 3 to 5 minutes the solution was changed to 540 mM NaCl 10 mM tris (0 Ca, 0 Mg). Patch pipettes contained 50 mM Na. Temperature was 4-7 degrees C. Following exposure to pronase (0.3 to 0.7 mg/ml for 30-60 seconds) two types of channels were observed; fast inactivation was eliminated in both cases. The more common variety (type I) has a single channel slope conductance (about 18-20 pS at -30 mV) and activation kinetics that are the same as measured from unmodified channels. At -30 mV their mean open time is approximately 0.4 msec, which is comparable to that found for channels with inactivation intact. The second variety of channel (type II) has a larger single channel conductance (about 30 pS) and much slower activation kinetics. Since channels with characteristics of type II were not seen without pronase treatment, it is presumed that they result from further modification of the sodium channel by pronase. Vertical calibration bars in the figure refer to single channel records.

Supported by NIH grant NS21111.

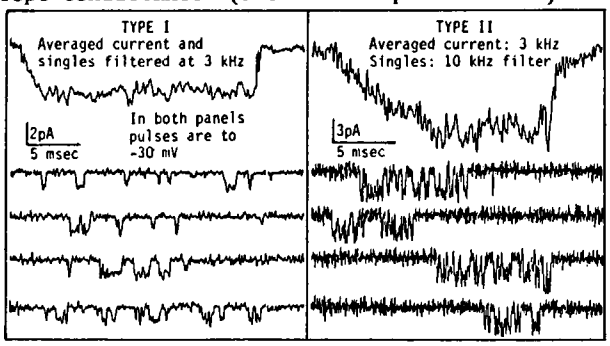

TU-AM-E2 PROPERTIES OF BTX-TREATED SINGLE Na CHANNELS IN SQUID AXON. *Ana M. Correa and F. Bezanilla.* Dept. of Physiology Yale University, New Haven, CT; Dept. of Physiology UCLA, Los Angeles CA and MBL, Woods Hole, MA.

We have used the modified cut-open axon technique to record single sodium channels from the internal surface of the squid giant axon. Axons were cut open in ASW (in mM: 440 Na, 50 Mg, 10 Ca, 10 TRIS) and the solution was changed to 540 NaCl, 10 TRIS with no added Ca or Mg. Batrachotoxin (BTX) was added to the patch pipette only or both to the bath and the pipette to a maximum concentration of 500 nM. Recordings were made at 5° C. Patches showed a variable number of channels, from 1 to several hundred. When BTX was only in the pipette normal channels became modified in a period of several minutes after seal formation and depolarization favored the transformation. In multichannel patches many channels remained unmodified. Modified channels had longer openings and lower conductance than normal channels. In 540 Na_o//45 Na_i (cation replacement was 145 mM N-methyl-glucamine) the normal channel had a slope conductance of about 20 pS and the BTX-modified channel had a slope conductance of 10 pS. In patches showing both normal and modified channels we separated them by holding the membrane potential at +100 mV for 4 min; upon returning to more negative holding potentials, BTX-treated channels behaved normally but unmodified channels were inactivated. The I-V curve was linear in 540 Na_o//514 Na_i and the single channel conductance was 10.5 pS for the modified channels. Analysis of a single-channel patch showed that the probability of being open vs. voltage, P(O), was sigmoidal with a value of 0.5 at around -80 mV, about 20 mV more negative than in normal Ca and Mg (Llano and Bezanilla, Biophys. J. 49:43a, 1986). The fitting of P(O) required at least 2 closed and 1 open states. Distribution of open times were well approximated by single exponentials in most of the voltage range; closed times required at least two exponentials as expected from a channel with more than one closed state. The voltage dependence is consistent with a gating charge with a valence between 3 and 4. Tetrodotoxin blocked the BTX-modified channels and the block was favored by negative holding potentials.

We thank Dr. J. Daly for providing BTX. Supported by USPHS grant GM30376.

TU-AM-E3 SINGLE-CHANNEL, MACROSCOPIC AND GATING CURRENTS FROM Na CHANNELS IN SQUID GIANT AXON
C. A. Vandenberg, & F. Bezanilla, Dept. of Physiology, UCLA, Los Angeles, CA 90024.

Sodium single-channel, macroscopic and gating currents were recorded with patch electrodes sealed to the intracellular surface of the squid giant axon using the modified cut-open axon technique. Patches contained up to several thousand Na channels. Patches with only one channel showed that an individual channel reopened several times before inactivating. Squid single Na channels had more rapid activation kinetics than mammalian neuronal Na channels, shorter open times, and appeared to reopen more often before inactivating. In the absence of added divalent cations (540 mM Na outside; 50 mM Na, 150 Cs inside), the single-channel current amplitude was approximately linear between -70 and +10 mV with a slope conductance of 20 pS (5°C). Under the same ionic conditions, the macroscopic instantaneous I-V in this range was linear, becoming slightly hyperbolic at more negative potentials. Macroscopic gating current also could be recorded with patch electrodes in the cut-open axon.

The effect of extracellular divalent cations on the ionic and gating currents was examined to develop a complete description of Na channel gating and to compare the single-channel currents recorded in the absence of divalent ions, with macroscopic ionic and gating currents measured in solutions containing Mg and Ca. Extracellular Ca and Mg in normal artificial sea water (440 mM Na, 50 mM Mg, 10 mM Ca) decreased the single-channel current amplitude, caused saturation of the macroscopic instantaneous I-V at negative potentials, and shifted the ionic current kinetics 10 to 20 mV towards more positive potentials. Experiments with axial-wire voltage clamp of dialyzed axons demonstrated that on-gating current also was shifted 10 to 20 mV towards more positive potentials. We conclude that the high concentration of extracellular divalent cations around the giant axon has a substantial influence on the sodium current amplitude, kinetics, and the action-potential threshhold due to a combination of rapid channel block and charge screening. (Supported by USPHS grant GM 30376).

TU-AM-E4 OPTIMIZED FUSION OF NATIVE OR RECONSTITUTED MEMBRANES TO ARTIFICIAL LIPOSOMES FOR SINGLE CHANNEL RECORDING Correa, A.M., Zhou, J.& Agnew, W.S., Cellular and Molecular Physiology, Yale Univ. Sch. of Med., New Haven, CT 06510

We report the efficient fusion of artificial liposomes with either native membrane vesicles or reconstituted liposomes containing purified ion channels, to produce structures suitable for patch clamp recording. Liposomes (PE:PS:PC, 5:4:1, for the reconstituted material, and PE:PS, 7:3, for native membranes) prepared in high ionic strenght buffer (400 mM NaCl, 10 mM Tris-HCl, 1 mM $CaCl_2$, pH 7.2) and sonicated to clarity are mixed with native or reconstituted membranes to final lipid and protein concentrations of 10 and 0.4 mg/ml, respectively. Samples must be briefly sonicated before being frozen at -80 °C and thawed at room temperature. Thawed samples contain bundle-like aggregates of multilamellar vesicles. Subsequent dilution in 250 mM NaCl, 10 mM HEPES, pH 7.2 causes vesicles to grow to final diameters averaging 30-40 μm. The morphology of the vesicle bundles and the efficiency of liposome expansion was dependent on protein concentration and PS content of the samples. The technique was used to record single channel currents from the purified reconstituted Na channel from Electrophorus electricus. Channels were purified by ion exchange and lectin affinity chromatography followed by removing detergent from lipid supplemented samples. Standard patch-clamp recording from excised patches treated with batrachotoxin (BTX) revealed 1-4 or more channels with characteristic BTX-modified properties. (Sigmoidal activation with voltage, γ ~ 10 and 16 pS). Efficiency of seal formation and seal resistance varied with ionic composition: 10-20 GOhm seals were readily formed in NaCl solutions. Fusion of native collagenased membranes from eel electroplax, or from rat skeletal muscle T-tubules permitted recording from excised patches. Intense channel activity observed indicated the presence of a variety of channels in these membranes. Supported by NS 17928 to WSA.

TU-AM-E5 SINGLE SODIUM CHANNELS IN RAT HEART AND RAT BRAIN HAVE DIFFERENT KINETIC PROPERTIES. G.E. Kirsch and A.M.Brown. Department of Physiology and Molecular Biophysics. Baylor College of Medicine, Houston TX 77030.

Tissue-specific differences between Na^+ channels of neuronal and cardiac origin are well known in regard to pharmacology and macroscopic gating. Here we extend the comparison to the single channel level. Na^+ channel gating was studied in neonatal rat ventricular myocytes and cortical neurons using gigaseal patch clamp methods under both cell-attached and excised patch conditions, at test potentials of -60 to -20 mV and at a temperature of 9-11° C. In both cell-attached and excised patches brain Na^+ channel mean open time progressively increased from less than 1 msec at -60 mV to about 2 msec at -20 mV. Near threshold, brain Na^+ channels exhibited single openings with dispersed latencies. In contrast, in cell-attached patches cardiac rat channel mean open time peaked near -50 mV, was three times brain Na^+ channel mean open time and declined continuously to a about 2 msec at -20 mV. Near threshold, cardiac Na^+ channels often opened in brief bursts and occasionally in prolonged bursts lasting tens of msec. In excised patches the frequency and duration of bursting increased and at -20 mV mean open times were prolonged showing that patch excision alters cardiac, but not brain Na^+ channel inactivation. These results show that cardiac and brain Na^+ channels can be distinguished by their microscopic properties. Whether these distinctions arise from different genetic messages remains to be established.

TU-AM-E6 KINETICS AND BLOCK OF SINGLE SODIUM CHANNELS IN VOLTAGE CLAMPED CARDIAC CELL MEMBRANES **Paul B. Bennett** Department of Pharmacology Vanderbilt University, Nashville, TN

Sodium channels were studied using whole cell and on-cell patch recording techniques in adult guinea pig and neonatal mouse and rat ventricular cells. Unitary conductance was determined by non-stationary fluctuation analysis and by direct observation of unitary current. In whole cell recordings from rat and mouse cardiocytes, fluctuation analysis of macroscopic Na current indicated a unitary slope conductance of 5.6 ± 0.32 pS (N=6) at potentials between -40 and +85 mV in 65 mM $[Na]_o$ at 16°C, corresponding to a unitary conductance of 12.9 pS in normal $[Na]_o$. In guinea pig ventricular cells using on-cell patches at 22°C, single channel Na current (i_{Na}) estimated from fluctuation analysis of multi-channel patches was compared to the unitary events in the same patches in 145 mM $[Na]_o$: i_{Na} was 1.4 ± 0.03 and 1.3 ± 0.26 pA at -40mV, respectively (chord conductances : 12.4 and 13 pS, respectively, assuming a resting potential of -70 mV and an $[Na]_i$ of 10 mM). Openings were brief (0.5±0.36 msec) and largely occurred near the beginning of a record. However, numerous late (>10 msec) openings, clustering together in bursts, were also observed. Lidocaine and its de-ethylated metabolite, glycylxylidide (GX) were studied by bath application. Lidocaine (80 μM) shifted the voltage dependence of Na channel availability to more negative membrane potentials by -11 mV and reduced the frequency of late channel openings, but had no effect on the unitary current amplitude. Like lidocaine, GX also inhibits Na currents in a use-dependent manner. After 10 pulses in 47 μM GX, the ensemble averaged Na current was reduced by 20%; the unitary current was not changed from control, but a reduction in open channel probability accounted for the reduction in the ensemble averaged current. These results demonstrate that lidocaine and GX inhibit macroscopic Na current without reducing i_{Na}. Furthermore, the equilibrium blocking reactions occur on a time scale similar to channel gating.

TU-AM-E7 EVIDENCE FOR A WATER-SOLUBLE FORM OF A TTX-INSENSITIVE Na-CHANNEL IN BULLFROG SKELETAL MUSCLE. E. Moczydlowski, J. Mahar and A. Ravindran. Dept. of Pharmacology, Yale Univ. School of Medicine, New Haven, CT 06510.

In pursuit of multiple Na-channel subtypes, we found two classes of high affinity binding sites for [^{3}H]STX in bullfrog skeletal muscle microsomes. One class exhibited high affinity for STX ($K_D \simeq 0.5$ nM), NEO ($K_D \simeq 0.1$ nM) and TTX ($K_D \simeq 1.3$ nM). The second class exhibited high affinity for STX ($K_D \simeq 0.1$ nM), lower affinity for NEO ($K_D \simeq 25$ nM) and complete insensitivity to TTX (tested up to 32 uM). The first class of binding sites corresponded to functional TTX-sensitive Na-channels that could be incorporated into planar bilayers. Surprisingly, the TTX-insensitive receptor for [^{3}H]STX was also present at nanomolar levels in the high-speed supernatant of soluble protein obtained after centrifugation at 180,000xg for 2 hr. The soluble receptor exhibited high affinity for STX ($K_D \simeq 0.1$ nM), lower affinity for NEO ($K_D \simeq 60$ nM), complete insensitivity to TTX (tested up to 80 uM) and a very slow rate of dissociation of [^{3}H]STX ($t_{0.5} \simeq 90$ min.) These phamacological properties are nearly identical to those of the membrane-bound, TTX-insensitive receptor. The soluble receptor has other unusual properties including a lack of binding competition between [^{3}H]STX and alkalai cations and adsorption to cation-exhange resins instead of anion-exchange resins, as found for conventional detergent-solubilized Na-channels. The toxin pharmacology of the soluble receptor is also similar to a functional Na-current previously described in bullfrog neurons and to a cytosolic receptor for [^{3}H]STX in frog heart reported previously [Doyle, D.D. et al., **Science 215:** 1117 (1982)]. Our results suggest that frog skeletal muscle contains both membrane-bound and soluble forms of a TTX-insensitive Na-channel. (Supported by AHA, Searle Scholars Program and NIH AR38796.)

TU-AM-E8 USE-DEPENDENT BLOCK BY TTX IN CARDIAC MYOCYTES. C.H. Follmer and J.Z. Yeh, Wyeth Labs, Philadelphia, PA and Northwestern Univ., Chicago, IL.

Isolated myocytes from cat atrium and ventricle were used to assess the steady state (s.s.) and use-dependent block of INa by TTX (1 μM). The INa availability curve was not affected when prepulses (pp) less than 300 ms were used but it was shifted by -7.5+1.7 mV when prepulses were 30 sec (n=3; V_h=-140 mV). The slope factor was unchanged. Use-dependent block was produced by prepulses as brief as 1 ms (Follmer and Yeh, 1986 Biophysics J. 49:294a, 1986). Recovery from block after a 1 ms prepulse (to -20 mV) showed that use dependent block actually developed during the recovery period at the holding potential (-120-140 mV). Recovery showed multiple phases; a fast phase to near complete recovery (98%), a slower net blocking phase to 72-82% of the prepulse current, and a very slow phase to complete recovery (10-20 sec.). Increases in the TTX concentration (1 to 2μM) increased the magnitude and onset of the net blocking phase. Prepulses that do not open channels required more than 1 sec to produce a net blocking phase during recovery. Pre-treatment with Chloramine-T removed fast inactivation of INa decay nearly completely but had no effect on the magnitude or time course of recovery after brief depolarizations. The results suggest that binding of TTX is slow, requiring several hundred ms in cardiac tissue (Carmeliet, 1987 Biophysics J. 51: 109-114, 1987), the s.s. block is voltage-dependent, and that fast inactivation is not required for steady-state or use-dependent block by TTX.

TU-AM-E9 ENHANCED TETRODOTOXIN SENSITIVITY OF SODIUM CHANNELS MODIFIED BY SEA ANEMONE TOXIN. Chau H. Wu, Department of Pharmacology, Northwestern University, 303 E. Chicago Avenue, Chicago, IL 60611

Previous studies have shown that the action potential plateau induced by sea anemone toxin (ATX) is more sensitive to the blocking action of tetrodotoxin (TTX) than the spike phase of the action potential. Preliminary results of computer simulations attribute this to the possibility that sodium channels modified by ATX may have a higher affinity for TTX than do unmodified channels. Therefore, we have performed TTX dose-response experiments on voltage-clamped crayfish axons to examine such a possibility. The TTX concentration used ranges from 0.1 nM to 10 nM. In normal axons sodium channels bind TTX with a K_D of 1.07 nM (at 10°C) as measured by the block of the peak sodium current. The toxin ATX-II from Anemonia sulcata induces a large steady-state sodium current that is contributed by non-inactivating sodium channels modified by the toxin. The modified channels are preferentially blocked by TTX with a K_D of 0.28 nM, representing a fourfold increase in sensitivity. The one-to-one stoichiometry remains unchanged. The modified channel also shows similar preferential sensitivity to saxitoxin. These results indicate that sea anemone toxin allosterically enhances the binding of TTX and STX to sodium channels.

TU-AM-E10 PURIFICATION OF THE TETRODOTOXIN RECEPTOR PROTEIN OF THE LOBSTER NERVE SODIUM CHANNEL. Raimundo Villegas, Françoise Sorais-Landáez, José M. Rodríguez-Grille and Gloria M. Villegas, Instituto Internacional de Estudios Avanzados (IDEA), Apartado 17606, Caracas 1015-A, Venezuela.

Solubilization and purification of the tetrodotoxin (TTX) binding protein of the lobster walking-leg nerve Na channel were carried out utilizing [^{3}H]TTX as a marker. The nerve membrane was solubilized with Lubrol-PX and the Na channel protein purified with DEAE Bio-Gel A, Bio-Gel HTP, and two Sepharose 6B columns. The lobster nerve Na channel was found to be more labile to solubilization and purification than the Na channel of vertebrates. Care was taken to keep the Na channel preparation as close to 1°C as possible and to use solutions (pH 7.5) containing Na channel protectors, i.e. egg phosphatidylcholine/Lubrol-PX mixture, TTX, EDTA, EGTA, PMSF, pepstatin A, iodoacetamide, antipain, phosphoramidon, soybean trypsin inhibitor, leupeptin and bacitracin. The [^{3}H]TTX specific binding of the Sepharose 6B fractions correlated with a large peptide of M_r 260K daltons (240-280K), though other peptides were also present in lesser amounts. From an initial binding value of 20.1 pmol of [^{3}H]TTX/mg of membrane protein for the solubilized membrane, the binding increased to 1241 pmol/mg of protein for the most active fraction.

TU-AM-E11 COCAINE-INDUCED CLOSURES OF SINGLE BATRACHOTOXIN-ACTIVATED NA^+ CHANNELS IN PLANAR LIPID BILAYERS. G.K. Wang, Department of Anesthesia Research Laboratories, Harvard Medical School/Brigham and Women's Hospital, Boston, MA 02115.

Batrachotoxin-activated Na^+ channels from rabbit skeletal muscle were incorporated into planar lipid bilayers. These channels appear to open most of the time at voltages larger than -60 mV. Local anesthetics, including QX-314, bupivacaine, and cocaine when applied internally, induce different duration of channel closures and can be characterized as fast (mean closed time at +50 mV <10 ms), intermediate (~80 ms), and slow (~400 ms) drugs, respectively. The bupivacaine and cocaine drugs appear to close Na^+ channels in an all-or-none manner. The action of these local anesthetics is voltage-dependent; larger depolarizations give rise to longer local anesthetic-induced closures. Both the dose-response curve and the kinetics of the cocaine-induced closures indicate that there is a single class of cocaine binding site. QX-314, though a quaternary-amine local anesthetic, apparently competes with the same binding site. External cocaine or bupivacaine application is almost as effective as internal application whereas QX-314 is ineffective when applied externally. Interestingly, external Na^+ ions reduce the cocaine binding affinity drastically whereas internal Na^+ ions have little effects. Both the cocaine association and dissociation rate constants are altered when external Na^+ ion concentrations are raised. We conclude that (a) one cocaine molecule closes one BTX-activated Na channel in an all-or-none manner, (b) the binding affinity of cocaine is voltage-sensitive, (c) this binding site can be reached by a hydrophilic pathway through the internal surface and by a hydrophobic pathway through the bilayer membrane, and (d) this binding site interacts indirectly with the Na^+ ions. A direct interaction between the receptor and Na^+ ions seems minimal. (Supported by NIH GM35401).

TU-AM-E12 DIVALENT CATION BLOCK OF NORMAL AND BTX-MODIFIED SODIUM CHANNELS IN SQUID AXONS. Joëlle Tanguy and Jay Z. Yeh. Lab. Neurobiologie Ecole Normale Supérieure, Paris, France and Dept. of Pharmacol., Northwestern Univ. Med. Sch., Chicago, IL 60611.

The ability of divalent cations to block Na channels was estimated from the instantaneous current-voltage curves (IIV) in internally perfused and voltage clamped squid axons. With an external solution containing 300 mM Na and 2 mM La and an internal solution containing 50 mM Na and 250 mM Cs, IIV was supralinear for inward current and sublinear for outward current. This IIV was not appreciably affected by the addition of 2-5 mM Ca to the external solution. Therefore, IIV obtained in nominal 0 or low Ca was taken as a control. The IIV was modified by addition of 30 mM divalent cations: the inward current was suppressed more markedly at more negative potentials, indicating a voltage-dependent block of the channels. The dissociation constants (K_d) at 0 mV estimated from IIV for Group IIA divalent cations were: Ca, 127 mM; Sr, 133 mM; Mg, 218 mM; and Ba, 370 mM and for transition elements were: Mn, 21 mM; Zn, 28 mM; Co, 38 mM; Cd, 41 mM; and Ni, 64 mM. All divalent cations showed a similar voltage dependence of block; their blocking site was estimated to be located at about one-quarter of the membrane field from the external side. BTX modification reduced the voltage dependence of the block by Ca, Sr, and Ba without affecting their Kd values , whereas it decreased the blocking potency of Mn, Zn, Co, and Cd by a fator of 2 to 3 with little effect on their voltage dependence of block. Thus, the difference in blocking potency among these divalent cations indicates that their blocking action does not arise from their screening effect of negative surface charges, but from their binding to a specific site within the channel. This site can be modified by BTX. Both hydration energy of divalent cations and their interaction with blocking site are of importance in determining their blocking potency. Supported by NIH grant GM-24866.

TU-AM-E13 SUBSTATE AND KINETIC CHARACTERISTICS OF DELTAMETHRIN-MODIFIED SODIUM CHANNELS. Kevin Chinn. Dept. of Med., Jefferson Med. College, Philadelphia, PA 19107.

Previous whole cell and single channel studies of Na^+ channels from mouse neuroblastoma N1E-115 cells have shown that the pyrethroid deltamethrin stabilizes several Na^+ channel states including 1) an open state, 2) a closed or inactivated state, 3) a substate and 4) a flickering state (Chinn and Narahashi, J. Physiol. 380:191; Biophys. J. 51:8a). The purpose of this study was to examine in detail the characteristics of deltamethrin-modified single Na^+ channels. The present studies revealed that channels could enter and leave several modified substates at -30 mV, having amplitudes 1/4 and 1/2 that of the main current amplitude as well as an approximately 3/4 amplitude substate, observed previously. At -100 mV, a 1/2 amplitude substate was found in addition to the 1/4 amplitude substate observed previously. The property of normal channels to remain inactivated for a prolonged period of time following a prolonged voltage pulse (slow inactivation) was examined in modified channels. The average number of channels opened per voltage pulse reversibly decreased (55%) when increasing pulse duration from 100 ms to 3 s, indicating that recovery of modified channels from inactivation depends on pulse duration. The effect of [deltamethrin] on observed channel states was tested. Using [deltamethrin] = 10 μM, only 2% of current traces had channels which flickered between the open and closed states, while flickering channels comprised 70% of observed channels when [deltamethrin] = 1nM (22°C). To summarize, the variety of deltamethrin-modified channel states includes substates having approximately 1/4 amplitude increments at -30 mV and -100 mV. The frequency of observing some of these states depends upon pulse duration or deltamethrin concentration. Supported by NIH grant BRSG 080-04605.

TU-AM-F1 STRUCTURAL CHARACTERIZATION OF THE 32 kDa SUBUNIT OF THE SKELETAL MUSCLE 1,4-DIHYDROPYRIDINE RECEPTOR. Alan H. Sharp, Mitchell Gaver, Steven D. Kahl and Kevin P. Campbell. Department of Physiology and Biophysics, University of Iowa, Iowa City, IA 52242.

The purified rabbit skeletal muscle dihydropyridine receptor contains four protein components of 175, 170, 52 and 32 kDa. The 170 kDa protein is the dihydropyridine binding subunit of the receptor (Sharp, et al. JBC (1987)262:12309). The 175 kDa protein is a glycoprotein that shifts in apparent molecular mass to 150 kDa on SDS-PAGE with reduction. To characterize the 32 kDa protein and determine its relationship to the other protein components of the purified receptor, we have raised polyclonal antisera against the various receptor components. Antisera directed specifically against the 175/150 kDa and 32 kDa proteins were produced by immunization of guinea pigs with individual bands of the purified receptor separated by SDS-PAGE under non-reducing conditions. Anti-175 kDa protein antisera did not react with a 32 kDa protein on immunoblots of reduced receptor resolved by SDS-PAGE suggesting that a 32 kDa protein is not disulfide linked to the 150 kDa protein, contrary to suggestions by another group. This was confirmed by SDS-PAGE of purified dihydropyridine receptor under non-reducing and reducing conditions. Anti-32 kDa protein antiserum was capable of immunoprecipitating receptor labeled with [^{3}H]PN200-110 suggesting that the 32 kDa protein is a component of the dihydropyridine receptor. The higher molecular weight proteins of the receptor were not labeled by anti-32 kDa protein antiserum on immunoblots showing that the 32 kDa protein is not a proteolytic fragment of the larger proteins. Immunoblots using antisera against the other components of the purified receptor also support the uniqueness of the 32 kDa protein. Therefore, our data indicate that the 32 kDa protein is a subunit of the dihydropyridine receptor and is distinct from the other subunits. (Supported by NIH HL37187)

TU-AM-F2 EFFECTS OF INTERNAL DIVALENT CATIONS ON SINGLE CALCIUM CHANNELS IN VASCULAR SMOOTH MUSCLE. N.B. Standen, J.F. Worley and M.T. Nelson. Department of Pharmacology, University of Vermont, Burlington, Vermont 05405.

Barium currents (80mM) through single calcium channels were measured in membrane patches excised from rabbit mesenteric artery smooth muscle cells. The internal surface of single calcium channels was exposed to 120 mM Na, 20 mM Cs, and 1 μM Bay K 8644 plus 0-10 mM cadmium, magnesium, lanthanum, and barium by moving the patch pipette through a series of flow pipes. Internal Cd, Mg, La in concentrations as high as 10 mM did not affect single calcium channel currents at 0 mV; mean unitary currents (±SE) in the control and in 10 mM internal Cd were 0.804 ± 0.057 pA and 0.798 ± 0.068 pA, respectively, (see Figure). In contrast, low concentrations of external cadmium (K_I = 50 μM) reduced high potassium-induced contractions of the same artery which are due to calcium entry through voltage-dependent calcium channels. Decreasing the barium driving force by elevating internal barium to 8 mM reduced the single channel currents by 27%. However, this reduction was greater than expected from constant field theory (10%). Single calcium channels appear to be remarkably insensitive to block by traditional inorganic blockers applied to the internal face of the channels.

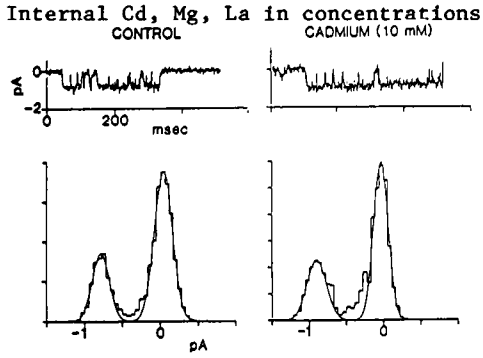

TU-AM-F3 ACTIVATION BY MEMBRANE POTENTIAL OF SINGLE CALCIUM CHANNELS AND NOREPINEPHRINE-INDUCED CONTRACTIONS IN RABBIT MESENTERIC ARTERY. J.F. Worley, N.B. Standen, J. Brayden and M.T. Nelson. Department of Pharmacology, University of Vermont College of Medicine, Burlington, VT 05405

Barium currents through single calcium channels, isometric contractions of isolated arterial rings, and membrane potential (Vm) were measured in rabbit mesenteric artery. Activation of single calcium channels in membrane patches was voltage-dependent, with a slope factor of about 7.5 mV. When Vm-dependent changes in inactivation and open Ca channel influx were taken into account, the voltage dependence of activation of contraction in K-depolarized arteries was the same as observed for single Ca channels. Norepinephrine (NE) at concentrations (< 5 uM) that did not depolarize shifted the relationship between Vm and contraction to more negative potentials without affecting the slope factor (see Figure). Bay R 5417 (50 nM), the stimulatory stereoisomer of the calcium channel agonist, Bay K 8644, also shifted this relationship to more negative potentials. These findings suggest that the voltage dependence of NE contractions is a direct result of the voltage dependence of calcium influx through calcium channels and that NE increases calcium channel open state probability without membrane depolarization.

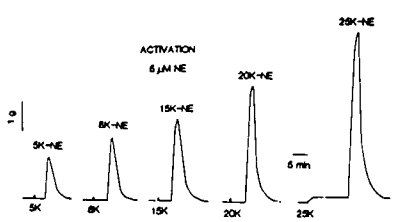

TU-AM-F4 ANTIBODIES AGAINST ADP/ATP CARRIER ENHANCE THE Ca^{2+} CURRENT IN ISOLATED CARDIAC MYOCYTES. M. Morad, N.W. Davies and H. P. Schultheiss. Dept. of Physiology, University of Pennsylvania, Philadelphia, PA & Dept. of Medicine I, University of Munich, FRG.

An antibody which inhibits nucleotide transport (ADP/ATP carrier) in the inner mitochondrial membrane (Schultheiss & Klingenberg, 1984. Eur. J. Biochem. 143,594) has been found in some cardiac disease states. We immunized rabbits with the isolated purified ADP/ATP carrier, and confirmed the specificity of the isolated antibody by showing that it binds to 30 KD band representing the isolated carrier. Exposure of isolated rat ventricular myocytes to the IgG fraction of the rabbit antisera led to saturable binding to the surface membrane, as detected with 125 I-protein A. The antibody binding was inhibited in a concentration-dependent manner, by pre-adsorption of the antibody on the isolated ADP/ATP carrier. In whole cell clamped isolated frog and rat myocytes addition of antibody led to the enhancement of Ca^{2+} current, measured using holding potentials of -50mv. Cells were dialyzed with Cs^{+} and $(Ca^{2+})_i$ was buffered to < 10-8M. Antibody enhanced ICa at all potentials tested. The enhancing effect was inhibited by nifedipine but was unaffected by B-blockers. Antibody also reversibly prolonged the action potential and enhanced contraction in frog ventricular strips. Exposure of rat myocytes to high concentrations of the antibody for 2-3 hrs led to time dependent cell deterioration. This effect was suppressed markedly in the presence of Ca^{2+} channel blockers. Our results suggest that a component of the antibody against ADP/ATP carrier cross reacts with the cardiac Ca^{2+} channel leading to its enhancement and eventual cellular Ca^{2+} overload.

TU-AM-F5 CALCIUM CHANNELS IN 3T3 CONTROL AND TRANSFORMED FIBROBLASTS. Chinfei Chen, Michael J. Corbley*, Thomas M. Roberts* and Peter Hess. *Depts. of Physiology and Neurobiology, and the *Dana Farber Cancer Institute, Harvard Med. School, Boston MA 02115.*

Recent evidence has implied that changes in cytoplasmic Ca^{2+} accompany the stimulation of DNA synthesis and cell proliferation in fibroblasts. We have previously characterized two types of voltage sensitive calcium channels in mouse 3T3 fibroblasts. The dihydropyridine (DHP) sensitive L-type Ca^{2+} channel activates at positive potentials and inactivates slowly, and the DHP resistant T-type Ca^{2+} channel activates at more negative potentials and inactivates within tens of milliseconds. If intracellular Ca^{2+} is involved in growth and proliferation, one would predict an abnormality in Ca^{2+} regulation in transformed 3T3 fibroblasts. Therefore, we have studied the whole cell Ca^{2+} currents of 3T3 fibroblasts transformed by activated c-H-*ras*, EJ-*ras*, v-*fms* and polyoma middle T oncogenes. These pilot studies have revealed that while the current densities for the L-type Ca^{2+} channel were not significantly different between normal and transformed cells, all tested transformed fibroblasts specifically lacked the T-type current found in all control 3T3 fibroblasts. Although the mechanism underlying the functional suppression of the T-type channel is unclear, these results imply that, like L-type channels, T-type channels are regulated by specific processes.

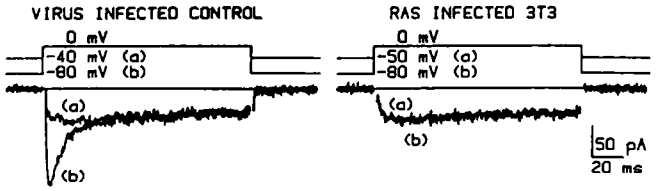

TU-AM-F6 **CALCIUM CHANNELS IN NERVE TERMINALS ISOLATED FROM RAT NEUROHYPOPHYSIS.** Martha C. Nowycky and José R. Lemos. Department of Anatomy, Medical College of Pennsylvania, 3200 Henry Ave. Philadelphia, PA 19129 and Worcester Foundation for Experimental Biology, 222 Maple Ave., Shrewsbury, MA 01545.

Multiple types of calcium channels exist in both peripheral and central neurons. While there is an absolute requirement for calcium entry in hormone secretion and neurotransmitter release, the type of calcium channel involved is still not established. To answer this question, we have performed patch clamp recordings on a preparation of nerve terminals isolated from the rat posterior pituitary (Cazalis et al., J. Physiol. 390, 55-70). These "neurosecretosomes" secrete oxytocin and vasopressin in a voltage- and Ca^{2+}-dependent manner.

Cell-attached patch clamp recordings were performed with 110 mM Ba^{2+} as the charge carrier, with TTX and TEA included in the patch pipette to block current flow through other channels. Under these conditions, we observe an inward current with a slope conductance of 28 pS. Channel activity is seen at test potentials positive to 0 mV and is not inactivated at relatively positive holding potentials. The reconstructed average current does not relax during a 136 msec pulse. In the presence of the dihydropyridine agonist, BayK 8644 (1 uM), channel openings are greatly prolonged. This channel appears to correspond almost exactly to the L-type, dihydropyridine-sensitive calcium channel described in chick dorsal root ganglion cells (Fox et al., J. Physiol., 1987).

In addition to the L-type calcium channel, neurosecretosomes have at least one type of smaller-conductance channel. Openings of this type of channel occur predominantly in the early part of the test pulse. Calcium channels in this preparation are being further characterized with a combination of single channel and whole cell recording techniques.

TU-AM-F7 BLOCK OF T-TYPE Ca CHANNELS IN GUINEA PIG ATRIAL CELLS BY CINNARIZINE. D.M. Van Skiver, Sherrill Spires and C.J. Cohen, Merck Inst. Ther. Res., Rahway, N.J.

T-type Ca channels were studied in guinea pig atrial cells using the whole cell configuration of the patch voltage clamp technique. T-type Ca channels deactivate much more slowly than L-type Ca channels, so total Ca channel current could be separated into 2 components by tail current analysis. T-type Ca channels inactivate rapidly, but recovery from inactivation is slow ($\tau \approx 0.5$ s at 22°C; $-100 < V < -60$ mV). The slow rate of recovery from inactivation may inhibit tachycardia originating in subsidiary pacemakers by slowing pacemaker depolarization. Several blockers of L-type Ca channels are also potent blockers of T-type Ca channels. The fig. shows the steady state voltage dependence of Ca channel block by cinnarizine. Block of both L and T-type channels increases in parallel with the degree of inactivation. The steady state voltage dependence of block indicates that cinnarizine preferentially binds to inactivated channels with $K_d \approx 0.9$ μM for both channel types. However, block of L-type channels is potent only when the cells are almost completely depolarized. At voltages where T-type channel availability is significant ($V < -50$), block of T-type channels is much more potent than block of L-type channels. Likewise, the Ca antagonists amiodarone and quinidine bind to inactivated T-type Ca channels with $K_d \approx 3$ and 40 μM, respectively.

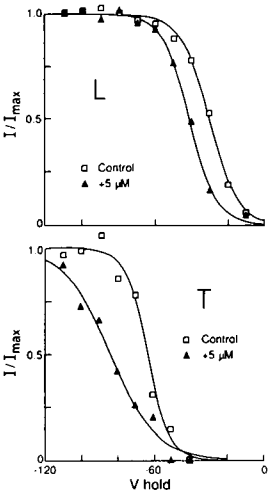

TU-AM-F8 HIGH AFFINITY AND TISSUE SPECIFIC BLOCK OF Ca CHANNELS BY FLUSPIRILENE. Sherrill Spires, D.M. Van Skiver, D.J. Plotkin and C.J. Cohen, Merck Inst. Ther. Res., Rahway, N.J.

Fluspirilene binds to a novel site on L-type Ca channels with high affinity (Galizzi et al., 1986; King et al., these abstr). Block of L-type Ca channels was studied with the whole cell configuration of the patch voltage clamp technique in GH_3 cells (derived from rat anterior pituitary) and in guinea pig atrial cells. In GH_3 cells, block is voltage dependent and increases in parallel with channel activation. The voltage and concentration dependence of block can be described by a model that postulates preferential binding to open channels; the K_d for binding to the open state is ≈ 0.5 nM. In atrial cells, fluspirilene either blocks the channels much less potently than in GH_3 cells ($\approx$ 100 fold) or increases L-type Ca currents. Increases in current were greatest in well polarized cells, so that the steady state availability curve was shifted to more negative potentials by fluspirilene. High affinity block of L-type Ca channels by nimodipine is similar in atrial and GH_3 cells ($K_d \approx 0.5$ nM). Studies with dihydropyridines support the idea that L-type Ca channels are similar in many tissues. In contrast, our studies with fluspirilene indicate that L-type Ca channels do not have a uniform pharmacology.

TU-AM-F9 MULTIPLE TYPES OF CALCIUM CHANNELS IN PC-12 CELLS GROWN IN THE ABSENCE OF NERVE GROWTH FACTOR. Mark R. Plummer, Diomedes E. Logothetis & Peter Hess, Dept. of Physiology & Biophysics, Harvard Medical School, 25 Shattuck street, Boston, MA 02115.

PC-12 pheochromocytoma cells are often used as a model for the study of excitation-secretion coupling as well as nerve growth factor-induced changes occurring during neuronal differentiation and neurite outgrowth. We have investigated Ca currents in the soma of non-differentiated PC-12 cells grown in the absence of nerve growth factor. Single channel recordings with 110 mM Ba as the charge carrier have revealed the presence of more than one type of unitary Ca channel activity. One type of channel has the unitary properties and pharmacological sensitivity of L-type Ca channels, whereas the other channel type shares some properties with the N-type Ca channel described in DRG neurons (Nowycky et al., Nature 316:440, 1985). Like its counterpart in DRG neurons, the second channel type in PC-12 cells requires negative holding potentials for maximal availability and its unitary conductance (16-19 pS) is smaller than that of the L-type channel (23-27 pS). Unlike the DRG N-type channel, however, the 16-19 pS channel in PC-12 cells may not inactivate completely at relatively positive holding potentials. The gating is characterized by a succession of bursts with brief openings and is active for longer times after patch excision than the L-type Ca channel.

TU-AM-F10 VERAPAMIL-SENSITIVE Ca^{2+} CHANNELS IN BONE CELLS. Sandra Guggino, Bertram Sacktor John Wagner, and Solomon Snyder. Laboratory of Biological Chemistry, Gerontology Research Center, NIA, NIH, Baltimore, MD 21224, and Department of Neurosciences, The Johns Hopkins University, Baltimore, MD 21205.

The osteoblast-like osteosarcoma cell line ROS 17/2.8 expresses a Ca^{2+} channel which carries 12 pS inward Na^+ current and 3-5 pS inward Ca^{2+} or Ba^{2+} current in cell-attached patches. The Ba^{2+}:Na^+ selectivity in excised patches is 1.3:1. The Na^+:K^+ selectivity is 1.4:1 calculated from the reversal potentials using the Goldman equation. Channel opening shows a dose dependent decrease in open probability (Po) and mean open time. 1,3,5,10 uM (+)desmethoxyverapamil (+DMV) causes a 14,66,83 and 93% respective decrease in Po. The (-)DMV isomer causes a 2-fold more potent decrease in open probability at 0 mV. The dihydropyridine agonists BAY K 8644 or (+)202-791 did not increase channel opening in the presence of Na^+ as the current carrying species. Homogenates of these cells exhibit saturable, stereoselective verapamil binding sites for (-)DMV and (+)DMV which have a Ki for ^{3}[H](-)DMV binding of 53 and 362 nM, with a maximal binding density of 5 pmoles/mg protein. Neither nitrendipine binding nor dihydropyridine-sensitive DMV binding was detected. ^{3}[H] DMV binding was inhibited 50% by 100-400 mM Li^+, Na^+, Cs^+, and K^+, by 1.7-5 mM amounts of Sr^{2+}, Ba^{2+}, Ca^{2+}, Mg^{2+}, as well as 0.6 mM amounts of La^{3+} Or Pb^{3+}. We conclude that osteoblasts in culture express a low selectivity Ca^{2+} channel which has phenylalkylamine but not but not dihydropyridine receptors.

TU-AM-F11 MODULATION OF CALCIUM TRANSIENTS AND CALCIUM CURRENTS IN CULTURED RAT MYENTERIC NEURONS BY NEUROPEPTIDE Y (NPY). L.D. Hirning, R.J. Miller and A.P. Fox, Department of Pharmacological and Physiological Sciences, University of Chicago, Chicago, IL 60637 (Introduced by S. Glagov).

The effects of NPY, a peptide neurotransmitter, were tested on calcium transients using the calcium indicator dye fura-2, and on Ca currents using whole-cell patch-clamp recordings. Brief exposure (60 sec.) of the neurons to elevated external K^+ (50 mM; bars beneath data trace in panel a) produced a large transient increase in $[Ca^{2+}]_i$, from basal levels of 30-50 nM to between 400-1500 nM after stimulation. $[Ca^{2+}]_i$ usually returned to resting levels 5-8 min after stimulation. NPY (100 nM), blocked a large fraction of the increase in $[Ca^{2+}]_i$ (as marked in panel a). On average, NPY reduced the responses to 61.9% (± 5.8%; n=14) of control. Pertussis-toxin pretreatment blocked the effects of NPY on the Ca^{2+} transients, indicating a G-protein link. The Ca currents, measured with 5 mM Ca (or Ba) as the charge carrier, appeared to have two components, an inactivating current which was more evident at negative holding potentials (HP= -80 mV; trace marked Δ in panel b) and a sustained current seen at depolarized HPs (- 40mV; not shown).

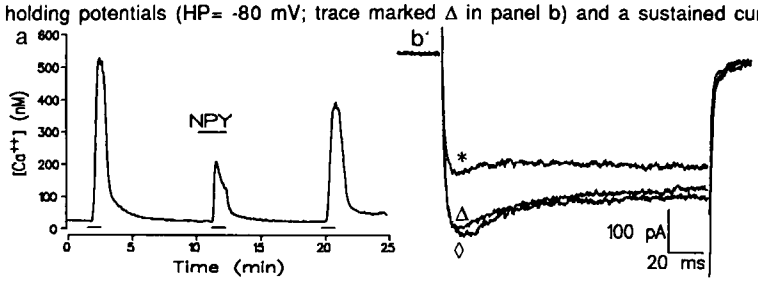

NPY (100 nM) produced a significant decrease in the Ca current (trace marked *), most evident on the inactivating component at HP= -80 mV, but also observed on the sustained current at HP= -40 mV. Interestingly, the currents recovered rapidly in the presence of NPY (trace marked ◊), suggesting desensitization. These data indicate that NPY inhibits Ca influx into myenteric neurons by blocking Ca channels, and that pertussis-toxin sensitive G-proteins may be involved.

TU-AM-F12 C-KINASE AND G PROTEINS MEDIATE INHIBITION OF Ca^{2+} CURRENTS BY NEUROPEPTIDE Y IN RAT DORSAL ROOT GANGLION NEURONS D. A. Ewald[1], R. J. Miller[1] and P. C. Sternweis[2] (Intr. by M. Makinen) [1] Dept. of Pharm. & Physiol. Sci., U. of Chicago, Chicago IL 60637 [2] Dept. of Pharm., U. of Texas Health Sci. Cntr., Dallas TX 75234

Neuropeptide Y (NPY), a neurotransmitter endogenous to the vertebrate spinal cord, can inhibit Ca^{2+} currents in cultured dorsal root ganglion (DRG) neurons. NPY inhibits both the sustained Ca^{2+} current evoked at 0 mV from a holding potential of -40 mV and the transient Ca^{2+} currents which are additionally evoked at 0 mV from a holding potential of -80 mV. (Whole-cell patch clamp with (in mM) 140 Cs, 10 EGTA, 1 Mg, 2 ATP and an ATP regenerating system in pipette and 10 Ca, 140 TEA and 1 Mg bathing the neurons.) Maximal effect was at10^{-7} M NPY and inhibition of both sustained and transient currents was observed (mean ± SE: 51.1 ± 3.1% and 61.4 ± 5.7%, N=8). We tested the possibility that activation of C-kinase by the second messenger diacylglycerol (DAG) is a necessary step in this inhibition by "down-regulating" DRG neurons for C-kinase by long-term pretreatment with phorbol esters (Matthies *et al.* J. Neurosci. 7 1198 '87). In down-regulated neurons the effect of 10^{-7} M NPY on sustained current was greatly diminished although the effect on transient currents was maintained (25.3 ± 2.1% and 63.4 ± 3.6%, N=8). This suggests that only inhibition of the sustained current involves DAG-activated C-kinase. Inhibition of Ca^{2+} currents by NPY was completely prevented by pretreatment with pertussis toxin (n=10). This implies that G proteins are involved in both the C-kinase mediated and the non-C-kinase mediated inhibitions. We tested the ability of G_o, a pertussis toxin sensitive G protein, to reconstitute the inhibitory effects of NPY by including its alpha subunit (α_o) in the patch pipette along with 1 mM GTP. Reconstitution of NPY-induced inhibition by α_o occured after a time delay of 5 to 15 min. With 10 nM α_o inhibition by NPY was reversible and increased with time. Maximum inhibiton on both sustained and transient currents was comparable to the effect of NPY on control neurons (44.8 ± 5.3% and 56.0 ± 2.4%, N=4). With 100 nM α_o inhibition was not readily reversed (45.5 ± 6.3% and 57.3 ± 6.9%, N=8). Thus α_o plus GTP can fully reconstitute PTX-sensitive inhibition by NPY. However the possibility that α_o is just mimicking the action of a different endogenous PTX substrate which normally plays this role has not yet been excluded.

TU-AM-F13 LHRH AND SUBSTANCE P INHIBIT N- AND L-TYPE CALCIUM CHANNELS IN FROG SYMPATHETIC NEURONS. K.R. Bley and R.W. Tsien (Intro. by R.L. Rosenberg). Dept. Cellular & Molecular Physiology, Yale Medical School, New Haven, CT 06510.

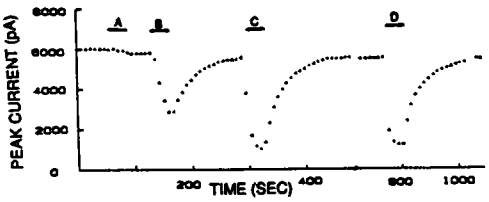

One of the best studied instances of ionic current modulation by peptides is the inhibition of M-current in bullfrog sympathetic ganglia by LHRH and substance P. We have tested whether these peptides also modulate calcium currents in dissociated sympathetic neurons from Rana catesbeiana and Rana pipiens. Whole-cell and single-channel recordings reveal that these cells have two types of calcium channels, similar to L- and N-type channels in dorsal root ganglion and rat sympathetic neurons (Lipscombe & Tsien, 1987). N-type channels produce a decaying current that undergoes steady-state inactivation at depolarized holding potentials, while L-type channels generate a long-lasting current that remains partially available even at -30 mV. We find that high concentrations of muscarinic agonists (A; 10μM muscarine) produce only negligible alterations of peak calcium current elicited during depolarizing steps from -90 to 0 mV, whereas application of 1 nM (B) and 5 nM LHRH (Chicken Type II) (C) and 500 nM substance P (D) profoundly inhibit the current in almost all cells. Similar inhibition occurs spontaneously when 50 μM $GTP\gamma S$ is added to patch pipette solutions. Since calcium current reduction occurs at all holding potentials, and high peptide concentrations can eliminate almost all inward current, both N- and L-type channels appear to be modulated. The second messenger mediating this response is unidentified, as neither activators nor inhibitors of protein kinases mimic the LHRH and substance P effect.

TU-AM-F14 DEVELOPMENTAL CHANGES IN Ca^{2+} CURRENTS FROM IDENTIFIED CHICK MOTONEURONS. D.P. McCobb*, P.M. Best#, & K.G. Beam*. Depts. of Physiology, *Colorado State University, Fort Collins, CO 80523, and #University of Illinois, Urbana,IL 61801.

Voltage-dependent Ca^{2+} currents in motoneurons are likely to be important regulators of neuromuscular system development, particularly since neuromuscular activity plays a prominent role in this development. Here we report on Ca^{2+} currents present at the earliest time at which chick spinal motoneurons can be identified by retrograde labelling techniques, embryonic day 6 (E6), and at a later stage (E11). A lipophilic dye (di-I) was injected into limb buds to label motoneuronal cell bodies in the spinal cord, which was dissociated 12-18 h later. The whole-cell patch clamp technique was used to measure Ca^{2+} currents (10 mM Ca^{2+} saline) in labelled motoneurons 24 h after dissociation. Based on kinetics and voltage-dependence, three distinct Ca^{2+} currents, comparable to the T,N, and L currents described in chick DRG cells by Nowycky et al. (Nature 316:440), were found in motoneurons from both E6 and E11 chicks. The percentage of neurons expressing T-type currents dropped from 87% at E6 to 37% at E11, while the percentage of neurons expressing N- and L-type currents increased from 89 to 95% and from 78 to 100%, respectively. N- and L-type current densities were found to increase from 2.37 ± 0.40 and 2.25 ± 0.55 pA/pF, respectively, at E6 (mean ± SEM) to 5.73 ± 1.10 and 5.84 ± 0.89 pA/pF, respectively, at E11. These results indicate that a variety of Ca^{2+} channels are expressed in motoneurons very early in development and that potentially important changes in their expression are occurring as the neuromuscular system matures. Supported by NIH grants NS24444 (KGB) and AR32062 (PMB).

TU-AM-G1 DIFFERENTIAL SCANNING CALORIMETRY OF THE UNFOLDING OF MYOSIN FRAGMENTS.
John W. Shriver, Irene Zegar, and Utpala Kamath. Department of Chemistry and Biochemistry, Southern Illinois University, Carbondale, Illinois, 62901.
The thermal unfolding of myosin fragments is being studied by differential scanning calorimetry. Heavy meromyosin (from a limited chymotrypsin digest of rabbit skeletal myosin) unfolds to give two endothermic peaks at 41°C and 48°C (in 25 mM TRIS, 0.1 M KCl, 5 mM $MgCl_2$, 1 mM DTE, pH 7.9). The low temperature peak is assigned to the subfragment-2 domain of HMM based on DSC scans of purified long subfragment-2. The unfolding of S-2 is reversible both in the isolated form and in HMM. The calorimetric and van't Hoff enthalpies of unfolding of the S-2 domain in HMM are essentially the same (190 $\pm$ 10 kcal/mol). The S-2 domain therefore unfolds under the above conditions as a single domain with no significant intermediates. In the presence of nucleotides, such as ADP, AMPPNP, and ADP with vanadate, the high temperature endotherm in the HMM scan shifts to higher temperature, indicating that the high temperature endotherm corresponds to the unfolding of the S-1 domain. This assignment has been confirmed by comparison with purified subfragment-1. The stability and thermodynamics of unfolding of the subfragment-2 domain in HMM is unaffected by the binding of nucleotide to the S-1 head. The unfolding of S-1 is irreversible making an analysis of the DSC data difficult. Methods for making the unfolding of S-1 reversible are being investigated (See Sabat and Shriver, this meeting). The unfolding of the proteolytic fragment light meromyosin has also been investigated. The unfolding of LMM is completely reversible and at least four domains are indicated. (Supported by NIH AR37174).

TU-AM-G2 DIFFERENTIAL SCANNING CALORIMETRIC (DSC) STUDY OF THERMAL UNFOLDING OF MYOSIN AND ITS SUBFRAGMENTS IN SEVERAL FORMS OF ASSEMBLIES. Antonio Bertazzon, Guang-hong Tian, and Tian Yow Tsong. Johns Hopkins University School of Medicine, Baltimore, Maryland 21205.

Rabbit myosin and its subfragments undergo multi-phasic helix-to-coil transitions in the range 40 to 70°C. They can be resolved into several quasi-two state transitions each representing the melting of an independent domain. This study examines the validity of such assumption and investigates the thermal stability of domains when myosin is assembled into filamentous structures. The result is summarized. 1) In agreement with Privalov & coworkers [Adv. Protein Chem. 35, 1 (1982)], the thermogram of rabbit myosin rod can be resolved into 6 quasi-two state transitions. At pH 7.0, the calorimetric ΔH for the transitions occurring at 42.2, 44.7, 46.4, 50.5, 54.8, and 55.1°C are, respectively, 201, 158, 238, 144, 163, and 124 kcal/mol. The total ΔH is 1050±50 kcal/mol. 2) The ΔH for each S1 is 265±12 kcal/mol and for each light chain is 143±30 kcal/mol. The sum of fragmente making up a myosin is 1870±50 kcal/mol, compared with the experimental value of 1920±130 kcal/mol for intact myosin, indicating that to the first approximation, these fragments melt independent of each other, the main difference being that the 54.8 and 55.1°C transitions of the rod occur a few degrees lower in myosin. 3) The surprise observation is that when myosin forms filaments, their melting behavior is greatly altered. The melting of domains becomes highly cooperative, i.e. the overall shape of thermogram is sharpened. The peak transition temperature is 50°C in 0.1 M KCl and reduces to 44°C in 0.2 M KCl. A clear correlation between transition temperatures and the states of myosin aggregation remain to be established. The study compares DSC thermograms with electron micrographs of myosin samples in different solvents and aggregation states.

[Supported by NIH Grant GM37304 to T.Y.T.]

TU-AM-G3 **SPECTROSCOPIC STUDIES OF VANADATE PROMOTED PHOTOCHEMICAL MODIFICATION OF MYOSIN SUBFRAGMENT- 1.** Christine R. Cremo, Jean C. Grammer and Ralph G. Yount, Biochemistry/Biophysics Program, Washington State University, Pullman, WA, 99164-4660.

Vanadate (Vi) is trapped at the active site of subfragment-1 (S1) as a complex with MgADP. Upon irradiation with near UV light, the complex dissociates and S1 is photomodified as evidenced by increased Ca^{+2} ATPase activity and a change in the UV absorption spectrum (Grammer and Yount (1987)*Biophys. J.* **51**, 25a). The difference absorption spectrum (photomodified minus control) has a maximum at 278 nm. The spectral differences in 4 M guanidine hydrochloride are large, representing an increase in optical density of about 15% or 10,000 l/mole-cm. The difference spectrum is pH dependent with a pK_a near 5.0. Further spectrophotometric studies have shown that the photochemical modification decreased the tryptophan fluorescence of S1 by 30%,suggesting the modification of one or two of the five tryptophans present in S1. Extensive proteolysis did not release the quenching of tryptophan fluorescence. ATP binding to the photomodified enzyme does not result in the increase in tryptophan fluorescence characteristic of native S1. However, analysis of the tryptophan content of photomodified S1 by (i) amino acid analysis after mercaptoethane sulfonic acid catalyzed hydrolysis and by (ii) colorimetric analysis with N-bromosuccinimide indicated no loss of tryptophan. The best evidence indicates that Vi promotes the photomodification of an amino acid residue close to tryptophan(s). This modified residue may then form an adduct with tryptophan to quench its fluorescence and to give increased UV absorbance. Studies are underway to identify the putative modified residue. Supported by grants from MDA and NIH (DK05195)

TU-AM-G4 PHOTOCHEMICAL CLEAVAGE OF MYOSIN SUBFRAGMENT 1 (S1) HEAVY CHAIN PROMOTED BY MG·ADP·VI TRAPPED AT THE ACTIVE SITE. Jean C. Grammer, Christine R. Cremo and Ralph G. Yount, Biochemistry/Biophysics Program, Washington State University, Pullman, WA, 99164-4660

Previous studies (see above abstact) have shown that UV irradiation of Mg·ADP·Vi trapped on skeletal S1 promotes the photochemical modification of S1. Although the S1 was modified, no cleavage of the protein chains was observed. In contrast, similar studies with sperm dynein (Gibbons et al. 1987, J. Biol. Chem. 262 2780) showed that both the α and β heavy chains undergo specific Vi dependent photocleavage. Here, it was possible to retrap Mg·ADP·Vi on the above photomodified S1 at levels ~ 80% of unmodified S1. Irradiation of the Mg·ADP·Vi complex on the previously photomodified S1 resulted in release of Vi and ADP as before. However, S1 now exhibited specific cleavage of the heavy chain to yield fragments of about 23 kDa and 75 kDa. These results suggest that cleavage is occuring near the consensus sequence of GXXGXGK (residues 178-184) in the heavy chain which may be part of the phosphate binding site. These results suggest Vi dependent photocleavage of peptide chains may be a two step reaction in which Vi has to bind twice to the same site to effect cleavage.
Supported by grants from MDA and NIH (DK05195)

TU-AM-G5 A KINETIC STUDY OF ADP-INDUCED DECREASE OF THE SH_1-SH_2 ENERGY TRANSFER DISTANCE OF MYOSIN SUBFRAGMENT-1. Frances Gonsoulin, Frank Garland*, and Herbert C. Cheung, Department of Biochemistry, University of Alabama at Birmingham, Birmingham, AL 35294 and Department of Natural Sciences*, University of Michigan-Dearborn, Dearborn, MI 48128

The resonance energy transfer distance between SH_1 and SH_2 of myosin subfragment-1 (S-1) is sensitive to MgADP. The nucleotide induces an increase in the transfer efficiency between donor 1,5-IAEDANS attached to SH_1 and acceptor DDPM linked to SH_2, and hence a decrease of the donor-acceptor separation by 7-8 Å (Dalbey, et al.(1983) Biochemistry 22:4696; Cheung, et al. (1985) Biochim. Biophys. Acta 832:52). We have investigated the kinetics of this ADP-induced change in energy transfer by following the decrease of donor intensity in stopped-flow experiments in 60 mM KCl, 30 mM TES, pH 7.5 and 20 °C. The experiments were carried out with doubly labeled S-1 in the range 2-20 μM and [ADP] from 10 to 1000 μM. None of the kinetic traces could be fitted to a single exponential, but they all could be fitted to a two-exponential model. The observed fast rate constant (k_1) increased with [ADP] from 1-2 s^{-1} to over 30 s^{-1}. The corresponding increase of k_2 was from ca. 0.2 to above 3 s^{-1}. The reaction was also monitored by fluorescence polarization. The results showed no change in polarization over the same time interval, suggesting that the increase in energy transfer arose from a decrease in donor-acceptor distance. The amplitudes of this signal change can be interpreted in terms of changes in donor-acceptor distance. Work supported in part by a grant from NIH (AR 31239).

TU-AM-G6 FLUORESCENCE ENERGY TRANSFER STUDIES OF THE ROLE OF C-PROTEIN IN THICK FILAMENT ASSEMBLY AND MYOSIN EXCHANGE A. D. Saad, E. Zlotchenko and I. Tan. Department of Cell Biology and Anatomy, Cornell University Medical College, New York, New York 10021.

A possible role of C-protein in thick filament assembly and stability was examined by comparing the assembly and exchange properties of myosin thick filaments in the absence and presence of C-protein. Chicken pectoralis myosin and C-protein were isolated and labeled with either donor (5-(2-((iodoacetyl)aminoethyl) aminonaphthalene-1-sulfonic acid) or acceptor (5-iodoacetamidofluorescein) fluorochromes. Polymerization of myosin into filaments was monitored using a fluorescence energy transfer (FET) assay (Saad, A. D. et. al (1986) Proc. Natl. Acad. Sci. USA 83:9483-9487). Donor labeled myosin and acceptor labeled myosin were mixed in high salt (0.5M KCl, 10mM Imidazole, pH 6.8) in the absence or presence of C-protein. Assembly was monitored by the decrease in donor fluorescence upon dilution into low salt (0.125M KCl, 10mM Imidazole, pH 6.8). The presence of C-protein did not effect the incorporation of myosin into thick filaments. Using a FET exchange assay the effect of C-protein on the ability of myosin to exchange between filaments was also examined. Myosin and C-protein were mixed (1:1 molar ratio) and copolymerized into filaments containing either fluorescently labeled myosin or labeled C-protein. Donor-labeled filaments were then combined with acceptor labeled filaments and exchange of either myosin or C-protein monitored. C-protein exchanged extensively and rapidly between filaments that contained both myosin and C-protein. Myosin exchange in these copolymers was significantly lower than that in filaments containing only myosin. These results suggest that C-protein may function as a stabilizer of myosin thick filaments. (Supported by NIH - AM37653 and New York Heart Assoc.)

TU-AM-G7 MODIFYING PRE-SELECTED SITES ON PROTEINS: APPLICATION TO THE 634-642 SEGMENT OF MYOSIN S-1 HEAVY CHAIN. Patrick Chaussepied, Tatsuo Maita, Genji Matsuda, Shigeo Kubota and Manuel F. Morales. CVRI, UCSF, San Francisco, CA 94143 and Nagasaki University, Nagasaki, JAPAN.

In order to study structure - function relationships within S-1 we are developing a novel method for specifically modifying preselected stretches of chain. Knowing the sequence in a stretch like 634-642, that is characterized by many lysines, we have synthesized a complementary peptide. This peptide is targeted because it bears a negative residue to go opposite to a positive of the protein, a hydrophobic opposite to a hydrophobic, etc. The peptide could be (and was) crosslinked to the target stretch with EDC in the presence of ATP, and carried a fluorescent reporter. 100% labelled S-1 could be isolated by DE-52 chromatography. Analysis with proteases showed the peptide to be at the expected site. Preliminary experiments show that Mg·ATPase of modified S-1 is essentially unchanged, while K-ATPase is slightly decreased. On the other hand, with actin-activated MgATPase, Vm was only 25% of control and the apparent affinity was about half of control. The Trp response to ATP was significantly reduced. Research supported by MDA fellowship, grants HL-16683, GM-10880, and NSF INT 8514204.

TU-AM-G8 CHARACTERIZATION OF THE ISOLATED AND RENATURED 23 kDa N-TERMINAL FRAGMENT OF THE MYOSIN HEAVY CHAIN. Andras Muhlrad. Hebrew University Hadassah School of Dental Medicine, Jerusalem, Israel and Cardiovascular Research Institute, University of California, San Francisco, CA 94143.

The 23 kDa fragment was isolated from the tryptic digest of rabbit skeletal myosin S-1 as follows. The heavy chain fragments were dissociated by 6M guanidine HCl and the 23 kDa fragment was precipitated by ethanol. The washed ethanol pellet was dissolved in 2% SDS and filtered through a Sephadex G-100 column. SDS was removed by ion exchange in the presence of 6M urea. The 23 kDa fragment was further purified on a QAE Sephadex G-50 column. Finally it was renatured by removing urea by dialysis in the presence of 0.2 M sucrose. The CD spectrum of the isolated fragment indicated that its structure was partially ordered. The tryptophan fluorescence emission spectrum of the fragment showed a substantial red shift on adding guanidine HCl, indicating that in renatured 23 kDa the tryptophans are located in a relatively hydrophobic environment. However both tryptophans of the fragment were accessible to acrylamide as shown by fluorescence quenching. The isolated 23 kDa fragment binds to F-actin, since it cosediments with actin and inhibited acto-(S-1)ATPase. The fragment does not have ATPase activity and it does not bind tightly the ring moiety of ϵ-ATP (it does not protect ϵ-ATP from acrylamide guenching). Actin binding by the fragment was also indicated by a nitrocellulose actin overlay method wherein a tryptic digest of S-1 is electrophoresed on a SDS-slab gel and transferred to nitrocellulose. The nitrocellulose is overlayed by tetramethyl rhodamine iodoacetate labeled F-actin. The fluorescence pattern indicated that actin was bound to both the 20 kDa and the 23 kDa fragments of S-1 heavy chain. The actin-overlay of a further cleaved 23 kDa fragment showed that an actin binding site resides on the C-terminal region of this fragment. This work was supported by grants from MDA, BSF, NSF and by HL-16683.

TU-AM-G9 PROTEOLYTIC CLEAVAGE OF MYOSIN HEAD DOMAIN JUNCTIONS ACTIVATES ACTIN SLIDING MOVEMENT *IN VITRO* Y.Y. Toyoshima, S.J. Kron, K.R. Niebling and J.A. Spudich Cell Biology, Stanford University School of Medicine, Stanford CA 94305

Biochemical studies of actin-myosin interaction have used proteolysis as a probe for the function of susceptible regions of the myosin molecule. We have applied this approach to determine the essential structures of the myosin molecule necessary for actin sliding movement. We have used an *in vitro* movement assay (Toyoshima *et al.*, *Nature* 328:536-539, 1987) to observe fluorescent actin filaments moving over nitrocellulose films coated with the proteolytic fragments of myosin. Intact myosin, chymotryptic HMM, papain S1, and chymotryptic S1 each support movement in this assay, yet at different characteristic speeds: 4, 7, 2, and 1 μm/s, respectively. Single-headed HMM produced by chymotryptic digestion of papain single-headed myosin supports movement at 11 μm/s. The different rates of the soluble fragments may reflect different modes of attachment to the nitrocellulose surface or may be due to intrinsic differences in chemomechanical properties. When papain S1 is trypsinized, two specific cleavages of the heavy chain occur which produce a species with very low actin affinity. The cleavage at the 50k/26k junction can be protected by actin. Trypsin-cleaved papain S1 and actin-protected cleaved S1 each supported actin sliding movements at rates higher than that of intact papain S1. Characterization of the specific cleavages responsible for the differing rates may implicate junctions between the myosin head domains in limiting the rate of myosin movement.

TU-AM-G10 BINDING AND REGULATION OF ACTOMYOSIN ATPASE. E. W. Taylor, University of Chicago

The inhibition of ATPase activity of striated muscle acto S1 (actin-tropomyosin-troponin-myosin subfragment-1) in the absence of calcium ion is determined primarily by a reduction in the rate constant of products dissociation (Chalovich and Eisenberg, J. Biol. Chem. 257, 2432, 1982). The rate constants of ATP and ADP dissociation are reduced by a similar factor (Rosenfeld and Taylor, J. Biol. Chem. 262, 4984, 9994, 1987). The binding of S1 or S1-ligand complexes is at least a two-step reaction $M.L + A \overset{K_1}{\rightleftharpoons} AM^1.L \overset{K_2}{\rightleftharpoons} AM^2.L \rightleftharpoons AM^2 + L$ where L is ATP, ADP, ADP.P_i, PP_i or no ligand (binding of S1 alone) and $K_1 = k_1/k_{-1}$. At low ionic strength k_2 is approximately 200 sec^{-1} for S1, S1.ADP and S1.PP_i. K_2 varies by 1000 fold for various ligands. In the $AM^1.L$ state actin is relatively weakly bound and K_1 varies about 50 fold for various ligands. In the absence of calcium k_2 is reduced by a large factor while K_1 is relatively unaffected (less than five fold). The results can be interpreted by a two-step binding mechanism, in which step 2 (the primary step in regulation) involves an interaction at a second region of the binding sites.

TU-AM-G11 HYDROLYSIS OF NUCLEOSIDE TRIPHOSPHATES BY ACTOMYOSIN-S1. H.D. White, X. Wang, and B. Belknap. Dept. of Biochem., E. Virginia Medical School, 700 Olney Rd. Norfolk, VA.

We have measured the steady state rates of hydrolysis of a series of nucleoside triphosphates by bovine cardiac and rabbit skeletal actomyosin-S1 and $K_{binding}$, the apparent equilibrium constant of S1 binding to actin during steady state hydrolysis. The dependence of the rates of hydrolysis of ATP, ε-aza-ATP, CTP, TTP, and UTP upon [Actin] are fit reasonably well by a hyperbolic curve. In contrast, the dependence of the rates of hydrolysis of ε-ATP, GTP and ITP upon [Actin] deviated strongly from a hyperbolic curve and are inhibited by [Actin] > $K_{binding}$. However, all of the nucleotides used had similar values for $K_{binding}$ and the differences between steady state kinetics of the two groups of nucleotides cannot be explained by differences in $K_{binding}$. Therefore, the rate of at least one of the attached crossbridge steps (possibly the hydrolytic step) must be considerably slower for GTP, ITP and ε-ATP. A similar non-hyperbolic dependence of rate upon actin concentration had been previously observed by Rosenfeld and Taylor for the hydrolysis of ε-ATP by rabbit skeletal actomyosin-S1. We have measured the rate of movement of fluorescent actin filaments with bovine cardiac HMM in collaboration with Steve Kron and Yoko Toyoshima in Jim Spudich's laboratory and the shortening velocity of rabbit psoas and soleus fibers with Ed Pate and Roger Cooke (see accompanying abstract) for the same series of nucleoside triphosphates. These results indicate that with the possible exception of ε-ATP the nucleoside triphosphates that have non-hyperbolic actin activation of hydrolysis support movement (and shortening) poorly, whereas, all of the triphosphates that have hyperbolic steady state kinetics support movement well. This work was supported by grants from the Muscular Dystrophy Association and the American Heart Association.

TU-AM-G12 EFFECTS OF ATP ON ACTO-S1 STEADY-STATE KINETICS AND THEIR RELATION TO THE ACTOMYOSIN KINETIC SCHEME. Marshall Balish and Paul Dreizen. Program in Biophysics, State University of New York Health Science Center at Brooklyn, New York.

We have previously reported that the striking inhibition of steady-state acto-S1 ATPase by excess ATP in the millimolar range can be attributed to multisite competitive inhibition of actin activation by free ATP. The previous studies were done using the LC1 and LC3 isoforms of rabbit fast-twitch muscle myosin S1 at relatively low actin concentrations (1 to 7 μM). Further studies at higher actin concentrations (4 to 50 μM) reveal profound increase of apparent Km for actin activation with increasing concentration of free ATP and also an apparent, though lesser increase of Vmax as free ATP is raised from 0 to 4 mM. A theoretical analysis of the four-state acto-S1 kinetic scheme,as proposed by Rosenfeld and Taylor (1984), shows that if the free ATP acts simply at several sites (away from the hydrolytic site) affecting only the acto-S1 interaction steps, then the apparent Vmz (as obtainedfrom extrapolation of double-reciprocal plots of velocity against actin concentration) should be depressed at low concentrations of free ATP, resulting in an increase of apparent Vmax with increasing ATP concentration. Theoretcial calculations predict this effect to be greater at higher actin concentrations and also greater for S1-LC1 than for S1-LC3, as here observed. A large increase of apparent Km is also predicted, consistent with the observed data. A similar analysis based on the six-state model using reported rate constants is more difficult to reconcile with the observed data on ATP effectson acto-S1 ATPase, at least in a simple way.